Bioactive Materials 31 (2024) 38–52

Contents lists available at ScienceDirect

Bioactive Materials

journal homepage: www.keaipublishing.com/en/journals/bioactive-materials

Bilayer vascular grafts with on-demand NO and H_2S release capabilities

Pengfei Li [a,1], Fubang Liang [b,1], Lijuan Wang [a,1], Dawei Jin [b], Yushuang Shang [a], Xu Liu [a], Yanjun Pan [b], Jiang Yuan [a,*], Jian Shen [a,c,**], Meng Yin [b,***]

[a] Jiangsu Collaborative Innovation Center of Biomedical Functional Materials, Jiangsu Key Laboratory of Bio-functional Materials, Department of Materials Science and Engineering, School of Chemistry and Materials Science, Nanjing Normal University, Nanjing, 210023, PR China
[b] Department of Cardiothoracic Surgery, Shanghai Children's Medical Center, School of Medicine, Shanghai Jiao Tong University, 1678 Dong Fang Road, Shanghai, 200127, PR China
[c] Jiangsu Engineering Research Center of Interfacial Chemistry, School of Chemistry and Chemical Engineering, Nanjing University, Nanjing, 210023, PR China

ARTICLE INFO

Keywords:
Small-diameter vascular grafts
Nitric oxide
Hydrogen sulfide
Keratin
Endothelialization

ABSTRACT

Nitric oxide (NO) and hydrogen sulfide (H_2S) gasotransmitters exhibit potential therapeutic effects in the cardiovascular system. Herein, biomimicking multilayer structures of biological blood vessels, bilayer small-diameter vascular grafts (SDVGs) with on-demand NO and H_2S release capabilities, were designed and fabricated. The keratin-based H_2S donor (KTC) with good biocompatibility and high stability was first synthesized and then electrospun with poly (L-lactide-co-caprolactone) (PLCL) to be used as the outer layer of grafts. The electrospun poly (ε-caprolactone) (PCL) mats were aminolyzed and further chelated with copper (II) ions to construct glutathione peroxidase (GPx)-like structural surfaces for the catalytic generation of NO, which acted as the inner layer of grafts. The on-demand release of NO and H_2S selectively and synergistically promoted the proliferation and migration of human umbilical vein endothelial cells (HUVECs) while inhibiting the proliferation and migration of human umbilical artery smooth muscle cells (HUASMCs). Dual releases of NO and H_2S gasotransmitters could enhance their respective production, resulting in enhanced promotion of HUVECs and inhibition of HUASMCs owing to their combined actions. In addition, the bilayer grafts were conducive to forming endothelial cell layers under flow shear stress. In rat abdominal aorta replacement models, the grafts remained patency for 6 months. These grafts were capable of facilitating rapid endothelialization and alleviating neointimal hyperplasia without obvious injury, inflammation, or thrombosis. More importantly, the grafts were expected to avoid calcification with the degradation of the grafts. Taken together, these bilayer grafts will be greatly promising candidates for SDVGs with rapid endothelialization and anti-calcification properties.

1. Introduction

Cardiovascular diseases (CVDs) are the leading cause of global mortality. Specifically, coronary heart disease is commonly treated with coronary artery bypass grafting. Due to the lack of suitable donor vasculature, approximately one-third of patients are non-eligible for autologous vessel grafting [1,2]. Artificial vascular grafts are considered to address the scarcity of autologous vascular grafts [3]. The large-diameter vascular grafts such as GORE-TEX® and Dacron (D > 6 mm) have been applied in clinics for decades. However, small-diameter vascular grafts (D < 6 mm) used as vessel replacements are not ideal due to thrombosis, intimal hyperplasia, calcification, and chronic inflammation caused by incomplete endothelium and abnormal proliferation of vascular smooth muscle cells (VSMCs) [4,5]. Endothelialization has been proven to be a promising strategy to improve the patency of small-diameter vascular grafts (SDVGs) [6,7].

Native endothelium consists of an endothelial cell monolayer that modulates vascular tone by releasing antithrombotic factors such as

Peer review under responsibility of KeAi Communications Co., Ltd.
* Corresponding author.
** Corresponding author. Jiangsu Collaborative Innovation Center of Biomedical Functional Materials, Jiangsu Key Laboratory of Bio-functional Materials, Department of Materials Science and Engineering, School of Chemistry and Materials Science, Nanjing Normal University, Nanjing, 210023, PR China.
*** Corresponding author.
E-mail addresses: jyuan@njnu.edu.cn (J. Yuan), jshen@njnu.edu.cn (J. Shen), yinmengmdphd@163.com (M. Yin).
[1] These authors contributed equally to this work.

https://doi.org/10.1016/j.bioactmat.2023.07.020
Received 14 June 2023; Received in revised form 23 July 2023; Accepted 24 July 2023

nitric oxide (NO), thrombomodulin, prostacyclin (PGl2), and tissue plasminogen activator [8,9]. The secreted NO plays a critical role in the cardiovascular system, including maintaining proper blood pressure, inhibiting platelet aggregation, promoting the proliferation of endothelial cells, and regulating smooth muscle cell behavior [10–12]. Consequently, SDVGs based on NO-releasing from exogenous donors or NO-generating from endogenous donors in the bloodstream by glutathione peroxidase (GPx)-like catalyst were developed to regulate vascular homeostasis and promote vascular remolding. Kabirian et al. 3D-printed vascular grafts with NO-releasing coating to mimic the native endothelium properties [13]. Bohl et al. incorporated three NO donors into polyethylene glycol hydrogels to inhibit the proliferation of smooth muscle cells and platelet adhesion [14]. Li et al. developed NO-releasing vascular grafts containing S-nitrosylated keratin to prolong the NO release period and achieve rapid reconstruction of the endothelial layer [15]. In comparison, the poor stability, short release period, and low NO capacity of grafts remain for vascular reconstruction. To overcome these limitations, NO-generating vascular grafts have been developed due to the long-term NO release period covering the complete revascularization process and stable release of NO. Endogenous NO donors such as GSNO and RSNO could be decomposed with GPx-like catalysts such as some metal ions [Cu(II), Zn(II), Fe(II), Co(II), and Ni(II)] and organoselenium to generate NO [16–18]. Among them, the Cu(II) ion is the most effective catalyst with GPx-like activity to generate NO from endogenous/exogenous donors. Zhang et al. incorporated copper-MOFs for sustained nitric oxide generation and long-term vascular patency [19]. Miao et al. fabricated copper-incorporated poly (ε-caprolactone)/keratin mats for tissue-engineered vascular grafts with the potential of catalytic nitric oxide generation [20]. More importantly, the release rate of NO can be regulated by adjusting the Cu(II) ion content, achieving controlled NO release.

As the third gasotransmitter after NO and CO, hydrogen sulfide (H_2S) also plays a significant role in the cardiovascular system, including protecting against cardiac hypertrophy, heart failure, myocardial ischemia, and atherosclerosis [21,22]. Similar to NO, H_2S exhibits potential therapeutic effects including anti-inflammation, angiogenesis, blood pressure regulation, and tissue remodeling [23–25]. Furthermore, H_2S has been reported as a strong antioxidant to protect EC from oxidative stress [16]. Zhao et al. demonstrated that ACS14 (aspirin-derived H_2S donor) with cytoprotective and anti-inflammatory capabilities could inhibit the adhesion and proliferation of VSMCs [26]. Longchamp et al. developed an H_2S-releasing hydrogel, which effectively inhibited the proliferation of VSMCs while facilitating the proliferation and transmigration of HUVEC in vitro [27]. In addition, H_2S can upregulate the expression of vascular endothelial growth factor of endothelial cells (ECs) and stimulate the angiogenesis process [28]. VSMCs are located in the medial layer of blood vessels, which play an important role in maintaining the elasticity, mechanical strength, and vasoactive responsiveness of the blood vessels. The abnormal proliferation and migration of smooth muscle cells are the pathological basis of hyperplasia and restenosis of vessels when the vascular system is damaged. One important strategy for vascular remolding is to regulate the abnormal migration and proliferation of VSMCs after graft implantation. VSMCs can produce H_2S to achieve blood pressure regulation and angiogenesis as well as reduce vascular hyperplasia and inflammation in the cardiovascular system [29]. The low levels of H_2S could effectively inhibit the proliferation of VSMCs and delay the hyperplasia in human veins.

Although H_2S and NO exert their effects via separate pathways, they act cooperatively to expedite angiogenesis, anti-inflammation, and vasodilatation [30]. H_2S is known to enhance the ability of NO to relax smooth muscle [31]. NO can increase H_2S endogenous production by elevating CSE and CBS expression in vascular smooth muscle cells [32]. Lee et al. reported that the co-release of NO and H_2S accelerated tube formation by HUVECs as compared to the single NO or H_2S-releasing groups in vitro [33]. However, the crosstalking between those two gasotransmitters in the cardiovascular system has not yet been revealed [34,35].

The artery consists of three layers, including the tunica intima, the tunica media, and the tunica adventitia. The intima comprises a single layer of endothelial cells (ECs) which act as a luminal barrier while providing cellular signaling to prevent thrombosis, infection, and inflammation. The media layer consists of a large number of circumferentially aligned VSMCs, elastic fibers, and ECMs, which provide sufficient mechanical strength and elasticity for blood vessels to maintain normal vascular contraction and relaxation under the action of blood pressure. Based on bionics, various vascular grafts have been prepared and explored for their potential in the treatment of CVDs. Vaz et al. produced a bilayered tubular scaffold of randomly oriented PCL nanofibers as the inner layer and aligned poly (lactic acid) (PLA) nanofibers as the outer layer to provide enough strength and compliance required for vascular applications [36]. Ye et al. fabricated a bilayered tubular scaffold consisting of PCL nanofibers in the inner layer and core-shell nanofibers encapsulating bovine serum albumin (BSA) and tetrapeptide in the outer layer to release BSA and tetrapeptide that could enhance cell growth [37]. He et al. fabricated heterogeneous porous bilayered nanofibrous vascular grafts by a two-step phase separation technique [38]. Mo et al. designed a bilayer vascular scaffold based on PLCL/collagen electrospun nanofibers and nanofiber yarns [39]. Yuan et al. developed bilayered grafts loaded with miR-126 and miR-145 by emulsion electrospinning [40]. David et al. and Mo et al. fabricated an elastomeric bilayered tubular structure using thermally-induced phase separation (TIPS) and electrospinning methods [41,42]. Zhang et al. prepared bilayer anticoagulant hydrogel tubes with PCL sheaths by freeze-thawing and electrospinning [43]. Yao et al. prepared gelatin@chitosan-heparin/polyurethane bilayered grafts by freeze-drying and electrospinning [44]. Wang et al. fabricated gelatin-heparin/polyurethane bilayer grafts by electrospinning technology [45]. Recently, Jin et al. combined electrospinning (inner layer) with rotary bioprinting (outer layer) to manufacture bilayer vascular vessels [46].

Inspired by the natural structure of blood vessels, dual NO and H_2S-releasing bilayer vascular grafts were developed by electrospinning (Scheme 1). The Cu(II) ions were fixed on the PCL mat to catalyze the generation of NO under physiological conditions and used as the inner layer of the grafts. Keratin-based H_2S donor was synthesized and electrospun with poly (L-lactide-co-caprolactone) (PLCL) to afford the outer layer of the grafts, which was capable to trigger the release of H_2S in the presence of glutathione (GSH). The surface morphology and chemical composition of the grafts were evaluated by scanning electron microscopy (SEM), attenuated total reflection Fourier transform infrared (ATR-FTIR) spectroscopy, and X-ray photoelectron spectroscopy (XPS). The released behaviors and the effect of NO/H_2S on the growth and migration of HUVECs and HUASMCs were investigated in vitro. Furthermore, a 3D-perfusion system was used to evaluate the endothelialization of HUVECs on the intima of grafts under flow shear stress. Finally, bilayer grafts were implanted and investigated in a rat abdominal aorta replacement model for 6 months to evaluate endothelialization and revascularization.

2. Results and discussion

2.1. Preparation and characterization of KAT

4-Aminobenzothioamide was conjugated with keratin to obtain a keratin-based macromolecular H_2S donor for the improvement of the poor stability and toxicity of small-molecular donors (Fig. 1A). The UV spectra were used to characterize the structure of keratin, 4-amiobenzothioamide (AT), and the KAT donor (Fig. 1A). The weak peak of KAT was shifted from 525 to 550 nm, indicating that AT was successfully linked with keratin. The H_2S releases of KAT and AT were investigated,

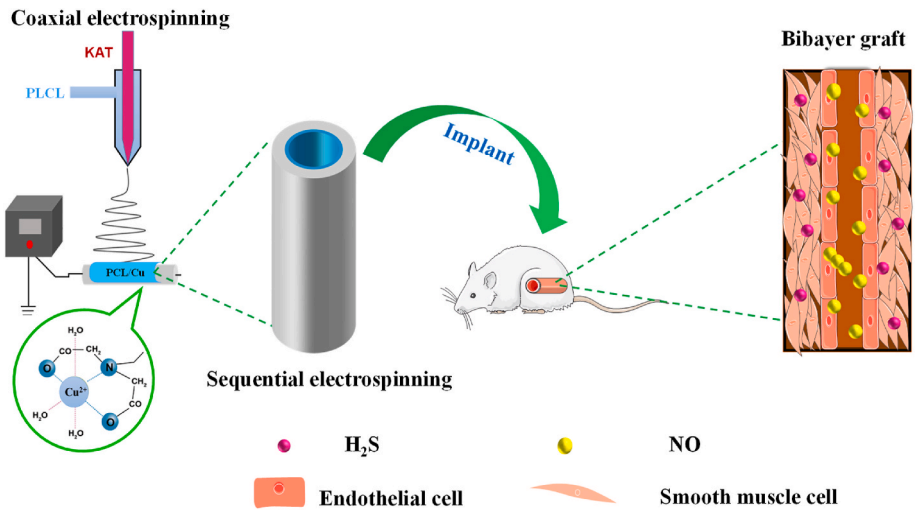

Scheme 1. Schematic fabrication of bilayer grafts through electrospinning with on-demand NO/H_2S releasing capabilities.

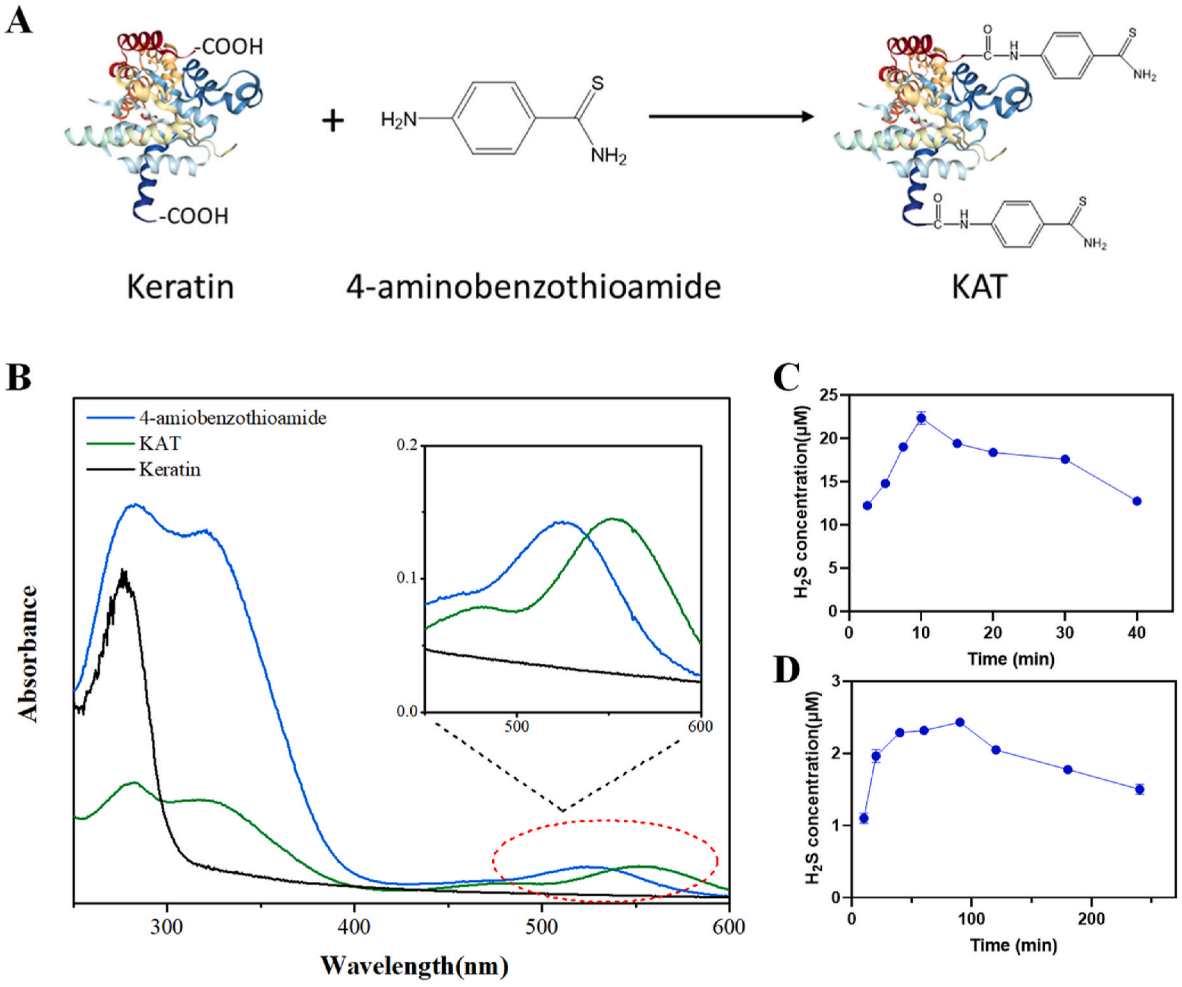

Fig. 1. (A) Schematic synthesis of 4-aminobenzothioamide conjugated keratin (KAT); (B) UV spectra of 4-amiobenzothioamide (AT), keratin, and KAT; (C) H_2S release profile of 4-amiobenzothioamide (AT); (D) H_2S release profile of KAT.

respectively. AT generated H_2S rapidly and reached a maximum after 12 min (Fig. 1C). In contrast, KAT generated H_2S slowly and reached the maximal concentration after 100 min (Fig. 1D). It indicated that the conjugation of AT with keratin prolonged the release of H_2S and improved its stability.

2.2. Preparation and characterization of PLCL/KAT-PCL/Cu grafts

PLCL/KAT-PCL/Cu grafts were fabricated with sequential electrospinning. For the inner layer, PCL was first electrospun, aminolyzed, and immobilized with iodoacetic acid for further chelating copper (II) ions

(Fig.S1). Aminolysis is one of the common strategies to improve the hydrophobic nature of PCL. However, excessive aminolysis would significantly reduce the mechanical strength. The effect of aminolysis time on the tensile strength of PCL mats was investigated. After treatment for 2 h with ethylenediamine, the tensile force of PCL was maintained at more than 80% of the initial tension. The mechanical strength was decreased sharply by less than 50% after treatment for 6 h (Fig.S2). To ensure enough mechanical strength, the aminolysis time of PCL was fixed at 2 h. The density of the amine group on the surface PCL mats was ca. 0.48 mmol/cm^2 by ninhydrin method (Fig.S3). Ethylenediamine tetraacetic acid (EDTA) is a polydentate ligand with six coordination sites that can capture metal ions to form chelates [47]. The aminolyzed PCL mats were modified by iodoacetic acid to form a structure similar to EDTA, which could also chelate metal ions to form the configuration of a hexatomic ring.

For the outer layer, the PLCL/KAT mats were prepared with coaxial electrospinning. PLCL is chosen in place of PCL due to its better elasticity, thereby avoiding the separation of two layers [48]. Also, good elasticity is conducive to improving the compliance of grafts. In addition, a core-sheath design provides a promising solution for controlling the initial burst release of drugs [49]. As shown in Fig. 2A, the XPS high-resolution spectra of N and Cu suggested aminolysis and Cu(II) immobilization on the surface of PCL. The chemical composition of PLCL/KAT was depicted in Fig. 2B. In comparison to PLCL, the peaks at 167 eV(S_{2p}) and 400 eV(N_{1s}) appeared, corresponding to the sulfur and nitrogen of KAT. In the high-resolution spectrum of sulfur, two peaks (162.6 and 167.8 eV) appeared on the PLCL/KAT mats, indicating the different chemical environments of sulfur. The peak of $S_{p1/2}$ at 162.6 eV was ascribed to sulfur within keratin, while the $S_{p3/2}$ peak at 167.8 eV was assigned to sulfur in 4-aminobenzothioamide.

ATR-FTIR spectroscopy was further used to investigate the chemical structures. The new peaks at 3500 and 3400 cm^{-1} were attributed to the asymmetrical stretching vibration absorption of primary amine, and the peak at 3300 cm^{-1} was the absorption of secondary amine (Fig. 2C). The above peaks vanished when the PCL-NH_2 was treated with iodoacetic acid, indicating that almost all amine groups were substituted with carboxyethyl groups. The strong absorption peaks at 1750 cm^{-1} of PLCL and PLCL/KAT were assigned to the symmetric and asymmetric stretching vibrations of carbonyl groups of PLCL bulk and keratin chain (Fig. 2D). The additional peaks at 1650 and 1540 cm^{-1} on PLCL/KAT were attributed to amide I and amide II of keratin.

The micromorphology of the PCL and PCL/Cu mats was observed by SEM(Fig.S4A and B). All the mats exhibited nanofibrous structures with interconnected micropores. There was no significant difference in the diameters of PCL(~0.9 μm) and PCL/Cu(~1.0 μm), indicating that the process of copper ion immobilization had no effects on the microstructure. SEM images of the PLCL and PLCL/KAT mats are shown in Figs.S4C and D. All the fibers displayed a smooth and continuous structure. According to the statistical data, the diameter of PLCL/KAT by coaxial-electrospinning was ca. 2.4 μm, which decreased slightly as compared with that of pristine PLCL. In addition, there were several well-distributing porosity structures, which would enhance nutrient penetration and cell infiltration. As a consequence, the hierarchical fibers within two different layers are beneficial to cell proliferation, thus speeding up the formation of biological blood vessels. The fluorescent microscope image demonstrated the core-shell structure of the PLCL/KAT nanofibers. The diameter of the core layer measured by ImageJ software was ca. 647 nm (Fig.S4E). The visible image of the PLCL/KAT-PCL/Cu bilayer grafts is shown in Fig.S4F.

The pristine PCL displayed a strong hydrophobicity, which would

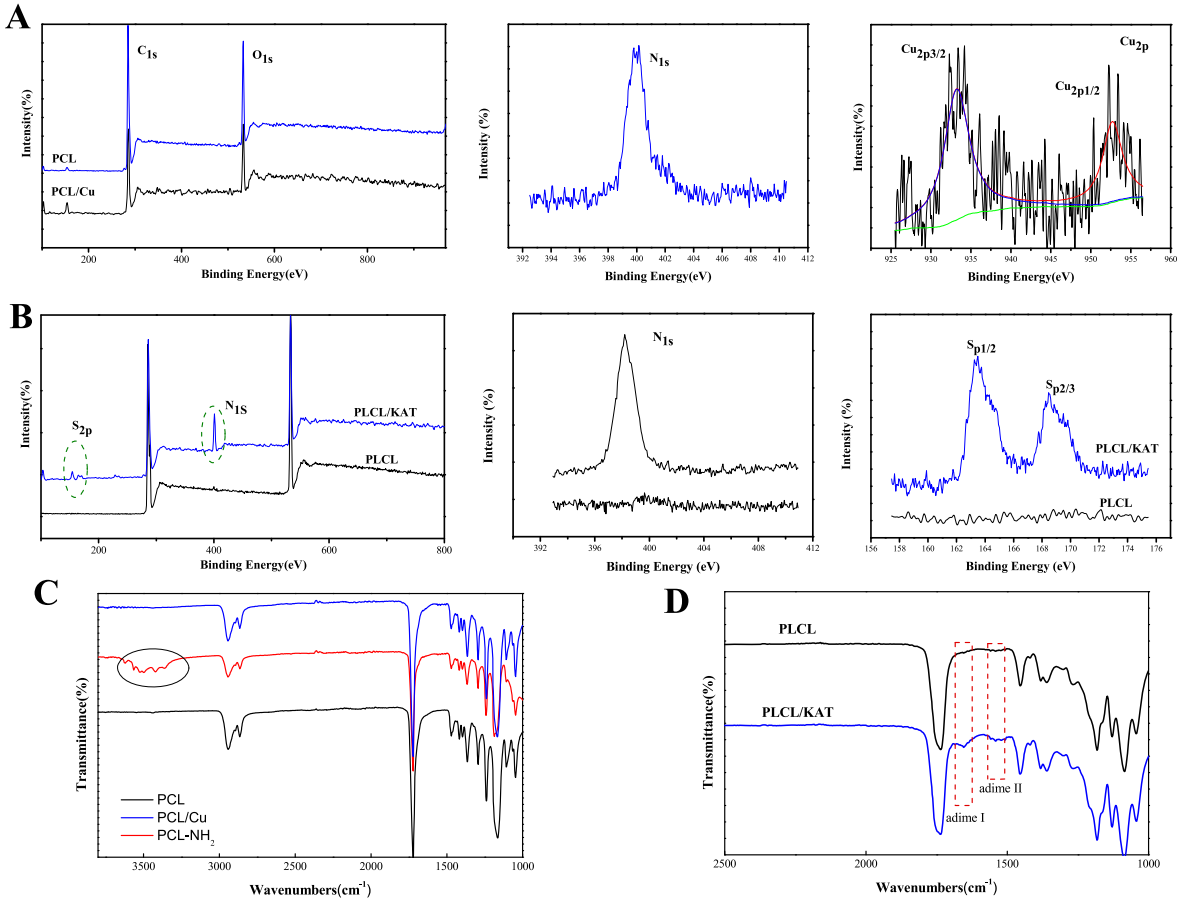

Fig. 2. (A) XPS spectra of PCL and PCL/Cu mats, and high-resolution spectra of N and Cu; (B) XPS spectra of PLCL and PLCL/KAT mats, and high-resolution spectra of S and N; (C) ATR-FTIR spectra of PCL, PCL-NH_2, and PCL/Cu mats; (D) ATR-FTIR spectra of PLCL and PLCL/KAT mats.

restrict the adhesion, migration, and proliferation of HUVECs(Fig.S5). The water contact angle (WCA) for PCL-NH_2 mats decreased significantly after treatment with ethylenediamine. Interestingly, a remarkably decreased WCA for PCL/Cu mats was attributed to the abundant carboxyl groups. These improvements are beneficial for the adhesion and proliferation of HUVECs. For PLCL/KAT mats, the WCA decreased slightly as compared with that for PLCL because most hydrophilic KAT was embedded in fibers as a result of coaxial electrospinning. These results further indicated the successful preparation of shell-core structural fibers.

2.3. Release of NO and H_2S in vitro

Copper is one of the most abundant trace elements in some proteins. Ceruloplasmin contains seven copper atoms and accounts for about 95% of the circulating copper in plasma [50]. Copper ions are known to catalyze the generation of NO from endogenous NO sources such as S-nitrosothiols [51]. Huang's group established a copper-dopamine coating on 316 L stainless steel by one-step assembly to endow the coating with in situ high NO catalytic capacity by decomposing RSNO endogenously existing in blood [52]. In addition, copper ions stimulate the proliferation of human endothelial cells [53,54]. However, the burst release of copper ions has the risk of endothelial cell cytotoxicity and vascular endothelial injury. Inspired by the chemical structure of EDTA, abundant amine and carboxyl groups were constructed on the PCL surface via ethylenediamine and iodoacetic acid to tightly chelate copper ions. As shown in Fig. 3A, PCL/Cu mats could effectively catalyze the GSNO to release NO sustainably. To verify the stability of copper ions, PCL/Cu mats were placed in a 50 μM EDTA solution for 30 min and then tested for the catalytic ability in the presence of GSNO. The PCL/Cu mats could still stably generate NO, suggesting that the copper ions were firmly fixed (Fig.S6).

Coaxial electrospinning is considered an effective strategy to achieve sustained drug release from core-shell nanofibers. Herein, the hydrophobic PLCL shell hindered the diffusion of cysteine residue compounds in plasma such as GSH, L-cysteine, and homocysteine to the core. In vitro results suggested that the release of H_2S was significantly prolonged to 240 h in the presence of GSH(Fig. 3B). It indicated that the PLCL/KAT layer was beneficial to improving the bioavailability of H_2S and regulating the behavior of vascular cells for a long term.

2.4. The proliferation of HUVECs and HUASMCs

Rapid endothelialization is an effective strategy for vascular grafts to reduce thrombosis and neointimal hyperplasia [55]. Local and continuous release of NO has been proven to be a potential and desirable strategy for blood-contacting implants [56]. Herein, the viability of HUVECs on PCL/Cu mats in the presence of GSNO was notably higher than that in the absence of GSNO, while those on PCL mats had no significant difference with and without GSNO(Fig. 3C). These results indicated that the PCL/Cu mats could generate NO to promote the growth of HUVECs effectively.

The abnormal proliferation of SMCs in damaged vascular walls is one of the key factors leading to intimal thickening and restenosis [57].

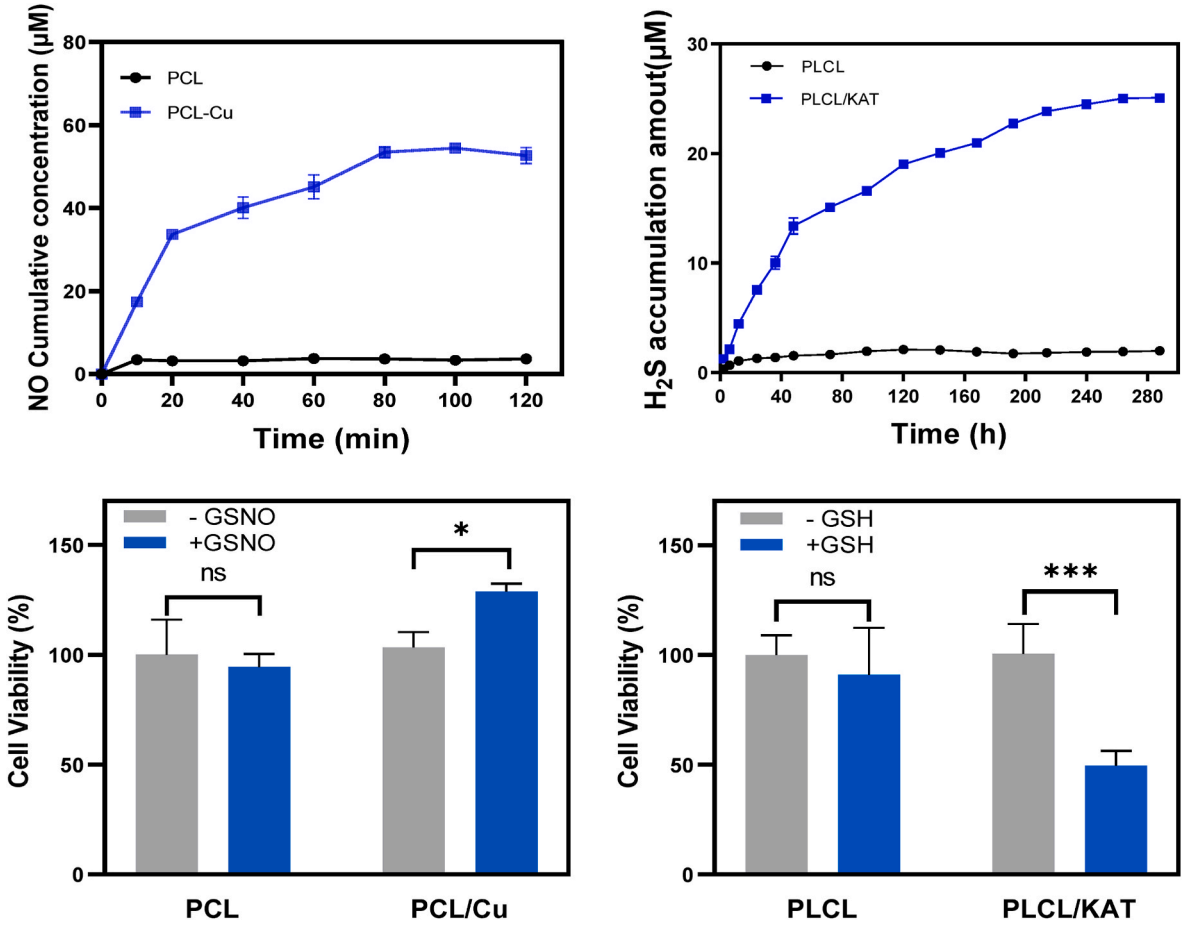

Fig. 3. (A) Cumulative NO release from PCL and PCL/Cu in the presence of GSNO(50 μM); (B) Cumulative H_2S release from PLCL and PLCL/KAT mats in the presence of GSH(1 mM); (C) Cell viability of HUVECs on PCL/Cu with and without GSNO(50 μM) for 3 d; (D) Cell viability of HUASMCs on PLCL/KAT with and without GSH (200 μM) for 3 d *indicates the significant differences between groups at $p < 0.05$, *** indicates the significant differences between groups at $p < 0.001$, and ns indicates no significant difference between groups.

Treatment with NaHS could significantly reduce the proliferation of SMCs and elevate the apoptosis of SMCs in the neointima [58]. Yang et al. found that the antiproliferative effect of H_2S was mediated via ERK and $p21^{Cip/WAK-1}$ activation. In addition, endogenous and exogenous H_2S could induce apoptosis of HUASMCs by upregulating caspase 3 and $p21^{Cip/WAK-1}$ through activation of ERK and p38 MAPK [59,60]. As depicted in Fig. 3D, the HUASMCs showed incremental proliferation on PLCL/KAT mats in the absence of GSH. The proliferation of HUASMCs was significantly inhibited in the presence of GSH, indicating the PLCL/KAT mats could control the proliferation of HUASMCs through the generation of H_2S. These results suggest that PLCL/KAT layer could prevent intimal hyperplasia after vascular implantation by inhibiting the proliferation of HUASMCs.

2.5. The migration of HUVECs and HUASMCs

The migration of vascular cells plays a vital role in vascular remolding after implantation [61]. The migration of endothelial cells can accelerate the formation of a natural barrier on the inner layer of grafts, which effectively inhibits blood coagulation. The migration of HUVECs on the PCL/Cu mats was evaluated in the presence of GSNO (Fig. 4A). The migration distance of HUVECs on PCL/Cu mats was significantly higher than that on PCL mats, indicating that the NO generated by PCL/Cu mats promoted the migration of HUVECs(Fig. 4B).

Smooth muscle cells can regulate vasodilation and contraction by releasing H_2S under normal physiological conditions [62]. After GSH was added, the migration distance of HUASMCs in the PLCL/KAT group decreased significantly as compared with that in the PLCL group, indicating that PLCL/KAT could inhibit the migration behavior of HUASMCs (Fig. 4C).

2.6. Co-culture of HUVECs and HUASMCs

Co-culture of HUVECs and HUASMCs was applied to mimic the

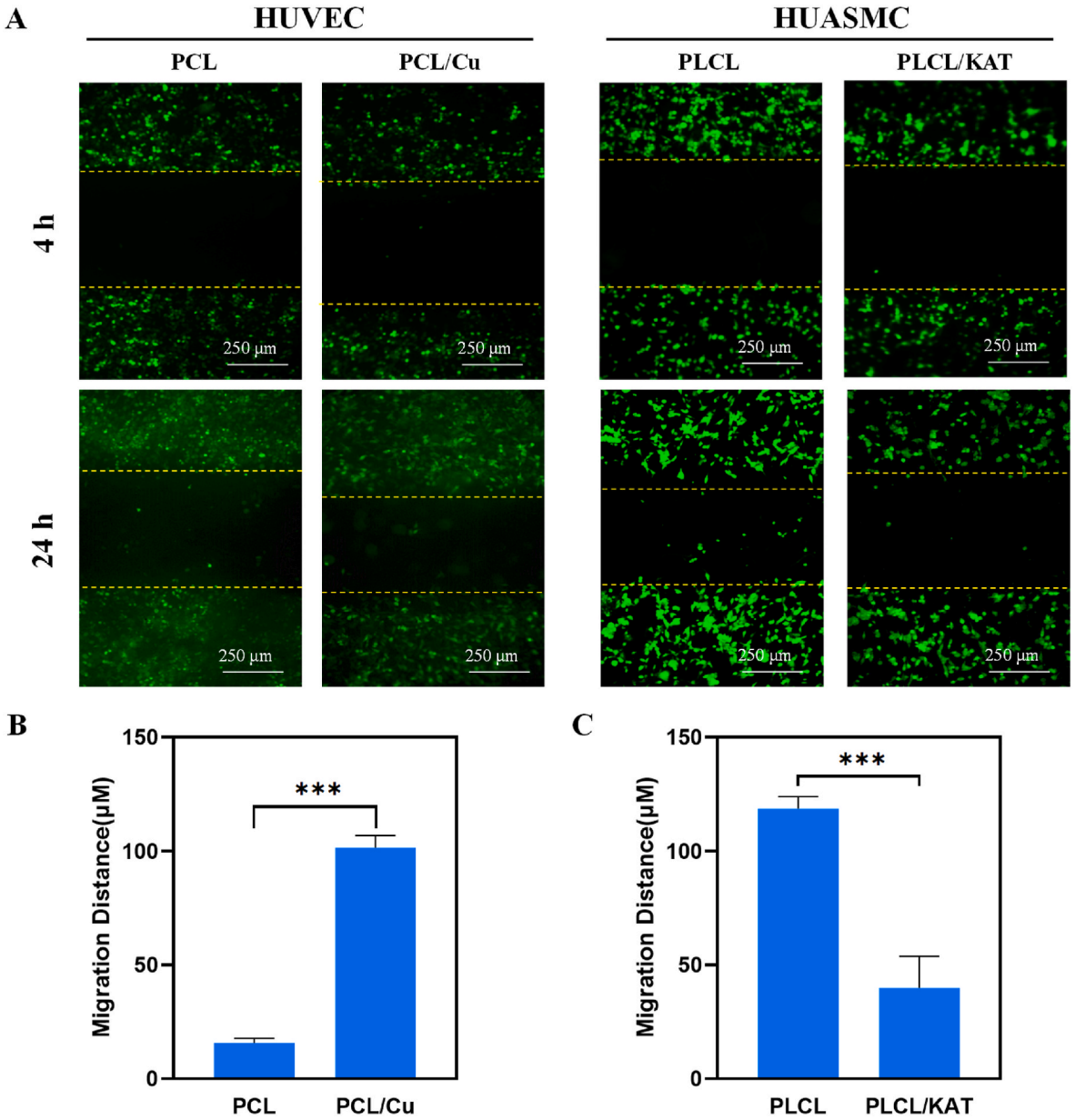

Fig. 4. (A) Fluorescent images of HUVEC on PCL and PCL/Cu with GSNO(50 μM), and HUASMC on PLCL and PLCL/KAT with GSH(200 μM); (B) Migration distance of HUVEC on PCL and PCL/Cu with GSNO(50 μM); (C) Migration distance of HUASMC on PLCL and PLCL/KAT with GSH(200 μM) (*** indicates the significant differences between groups at $p < 0.001$).

actual situation of grafts. After 4 h of incubation, a few HUVECs and HUASMCs adhered on mats in two groups (Fig. 5A). There was no significant difference between the two groups, indicating that these mats displayed no selectivity for both HUVECs and HUASMCs(Fig. 5B). After 24 h in PCL group, the ratio of HUVECs and HUASMCs was ca. 0.6, demonstrating that HUASMCs grew better than HUVECs. Interestingly, the ratio increased remarkably to ca.1.5 in PLCL/KAT-PCL/Cu group. These results suggested that bilayer PLCL/KAT-PCL/Cu mats had selectivity for HUVECs over HUASMCs due to the generation of NO and H_2S. Such desirable cell selectivity was beneficial to forming a confluent endothelial layer, facilitating rapid re-endothelialization, and alleviating neointimal hyperplasia without obvious injury, inflammation, or thrombosis.

2.7. Synergistic effects of dual NO and H_2S

2.7.1. Effect of H_2S release on NO secretion of HUVECs

NO and H_2S not only directly interact to regulate the cell behaviors of HUVECs and HUASMCs but also promote each other's expression through the corresponding pathway. The secretion of NO is one of the important markers of endothelial cell function recovery. As shown in Fig. 6A, the cumulative release of NO increased with the culture time, indicating that the release of H_2S by PLCL/KAT promoted the secretion of NO from HUVECs. H_2S can promote the secretion of VEGF and NO by HUVECs. In addition, the reduction environments provided by H_2S can prevent the oxidation of NO, as a result, prolong the half-life of NO [63, 64].

2.7.2. Effect of NO release on the H_2S secretion from HUVECs

Similarly, the secretion of H_2S by HUASMCs was significantly increased, indicating that the release of NO promoted the expression of

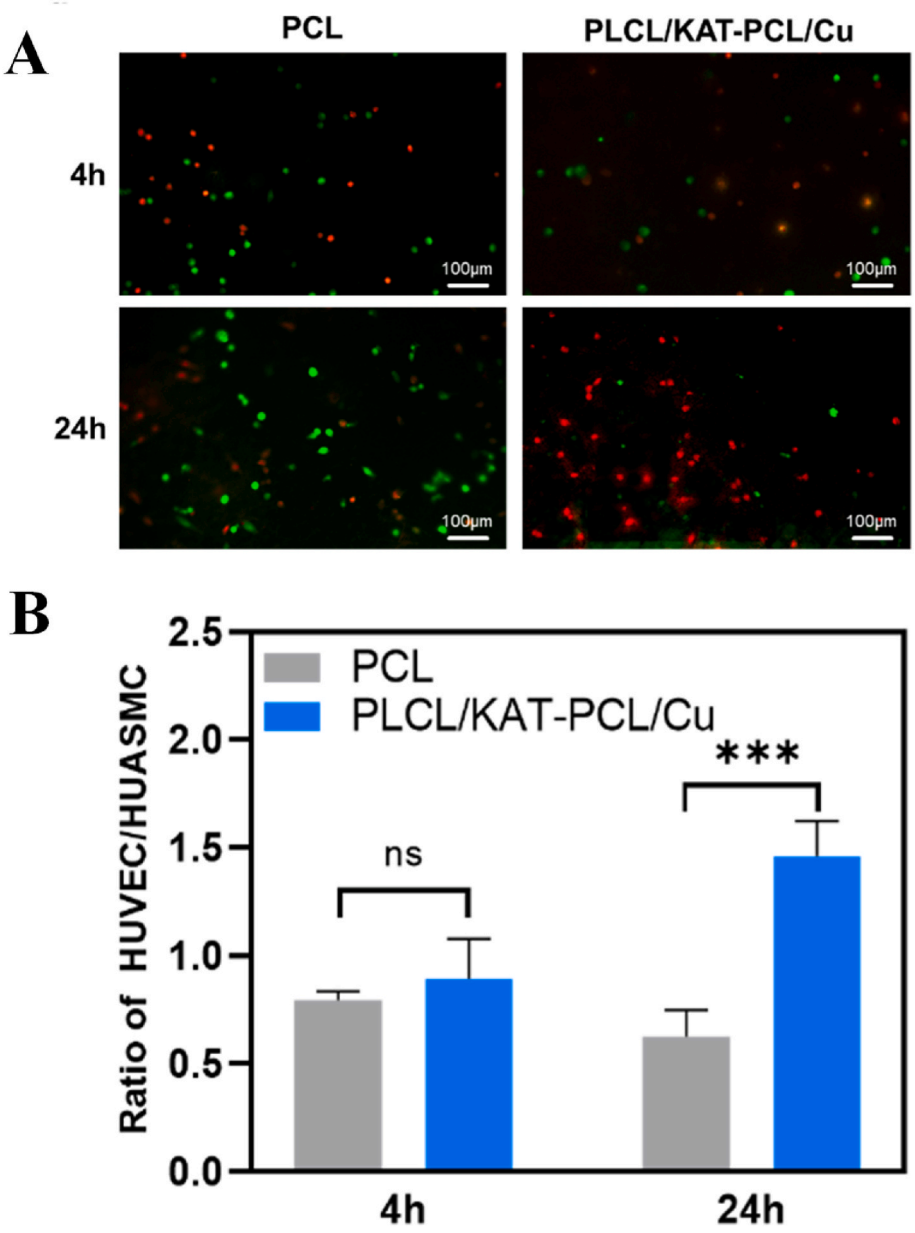

Fig. 5. Co-culture of HUVECs and HUASMCs on PCL and PLCL/KAT-PCL/Cu. (A) Fluorescence images of HUVECs (red) and HUASMCs (green) after co-culturing on PCL and PLCL/KAT-PCL/Cu; (B) The ratio of HUVECs and HUASMCs number on PCL and PLCL/KAT-PCL/Cu. The number was determined by at least four images by ImageJ, *** indicates the significant differences between groups at $p < 0.001$, and ns indicates no significant difference between groups.

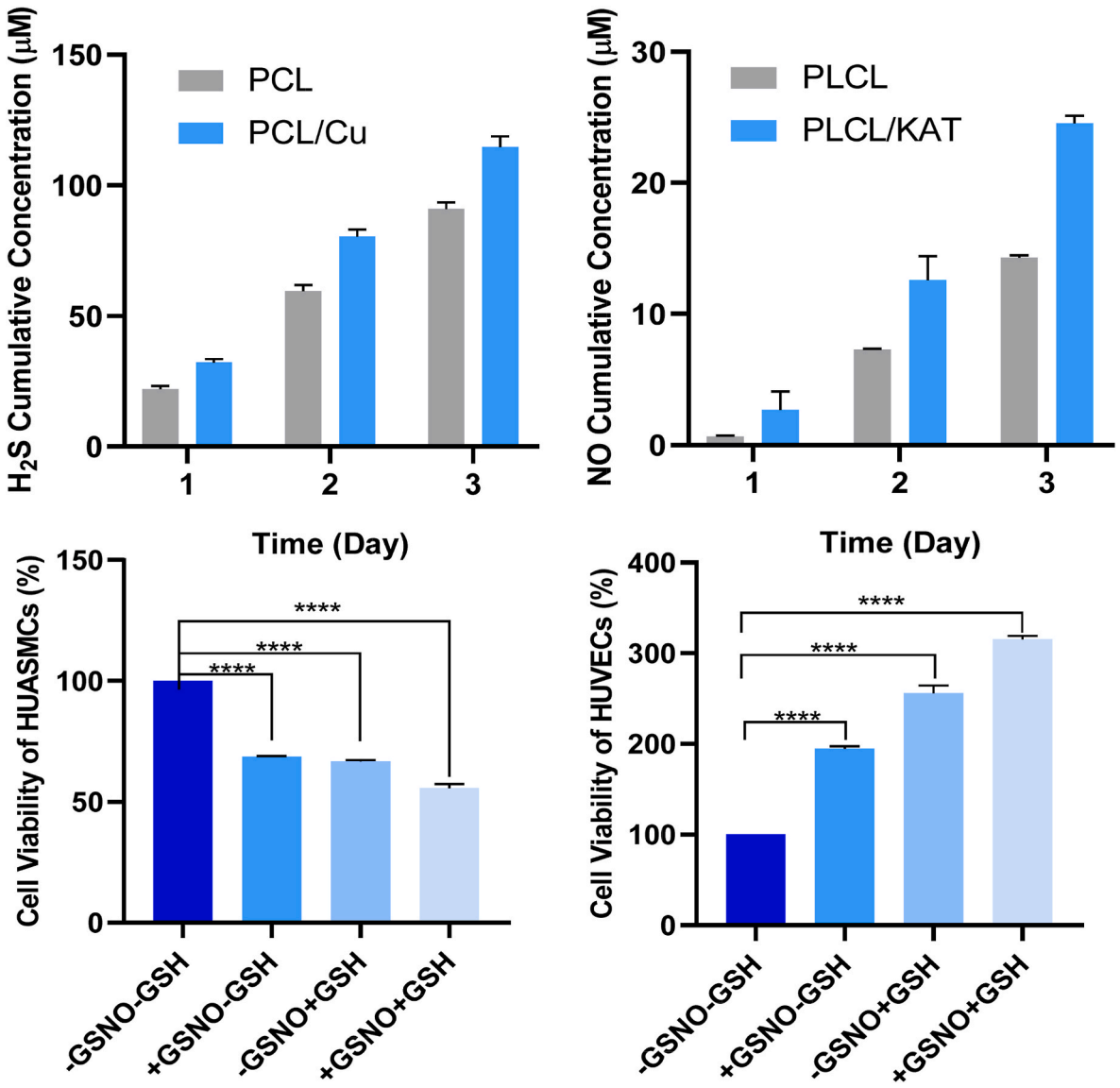

Fig. 6. (A) Cumulative release of NO from HUVECs on PLCL/KAT mats from 1 to 3 days (200 μM GSH); (B) Cumulative release of H_2S from HUASMCs on PCL/Cu mats from 1 to 3 days (50 μm GSNO); (C) The proliferation of HUVECs on PLCL/KAT-PCL/Cu mats for 2 days (200 μM GSH and 50 μm GSNO); (D) The proliferation of HUASMCs of HUVECs on PLCL/KAT-PCL/Cu mats for 2 days (200 μM GSH and 50 μm GSNO) (**** indicates the significant differences between groups at $p < 0.0001$).

H_2S from HUASMCs(Fig. 6B).

2.7.3. *Proliferation of HUVECs and HUASMCs*

The releases of dual NO and H_2S on HUVECs were first exploited (Fig. 6C). When GSNO and GSH were separately added, the proliferation of HUVECs in the PLCL/KAT-PCL/Cu group was promoted due to the release of NO and H_2S, respectively. Further, when GSH and GSNO were both added, the proliferation of HUVECs was enhanced as a result of the dual releases of NO and H_2S.

The migration of SMCs to the intima is the main cause of vascular stenosis. The effects of dual NO and H_2S on the inhibition of HUASMCs were also conducted (Fig. 6D). After the single addition of GSH and GSNO, the proliferation of HUASMCs in the PLCL/KAT-PCL/Cu group was inhibited due to the regeneration of NO and H_2S, respectively. Further, when both GSH and GSNO were added, the proliferation of HUASMCs in the PLCL/KAT-PCL/Cu group was significantly suppressed as a result of the dual releases of NO and H_2S. It indicated that the inhibition of HUASMCs could be enhanced by the combined actions of NO and H_2S. These results suggested that the bilayer mats could effectively regulate vascular cells through the synergistic effect of NO and H_2S, contributing to the reconstruction of blood vessels.

H_2S and NO regulate cell proliferation and migration via independent signaling pathways in the cardiovascular system. NO can promote the generation of H_2S from vascular tissues by up-regulating cystathionine-γ-lyase (CSE) expression [64,65]. In turn, H_2S can increase the NO production of endothelial cells by activating endothelial nitric oxide synthase (eNOS) [66,67]. H_2S inhibits rat VSMC proliferation and migration by promoting iNOS expression and NO generation. There is evidence that these two gasotransmitters interact in many ways with each other in biosynthesis and physiological reactions [35]. Especially, H_2S can contribute to angiogenesis and vasorelaxation as an enhancer of vascular NO signaling [68]. Hosoki et al. found that H_2S induced much stronger vascular relaxation in the presence of NO [31]. Therefore, the synergistic effect of NO and H_2S had great potential for vascular remolding. However, the crosstalking between H_2S and NO in the cardiovascular system has not yet been revealed [34,35]. In addition, the reaction between H2S and NO may form active intermediates that inhibit the proliferation of HUASMC [64,69].

2.8. Immunofluorescent staining for F-actin of HUVECs

As one of the most prominent cytoskeletal proteins, filamentous actin (F-actin) plays a critical role for HUVECs in responding to modulate cell alignment and maintain endothelial barrier function [70]. NO can regulate both the F-actin cytoskeleton and endothelial cell membrane stiffness [71]. F-actin stainings of HUVECs on PCL and PCL/Cu mats in the presence of GSNO are shown in Fig. 7A. The cytoskeleton of HUVECs in the PCL group was fuzzy, and the cell spread area was relatively narrow. In comparison, HUVECs in PCL/Cu group spread well on the collagen lumen. Furthermore, the cytoskeleton was clear, and F-actin was significantly thickened. These results demonstrated that the generated NO from the PCL/Cu layer promoted the viability and migration of HUVECs, resulting in rapid endothelialization of the vascular intima.

2.9. 3D-perfusion circuit culture

During the endothelialization process, the grafts are continuously exposed to fluid shear stress generated by the pulsatile flow of blood after implantation. Shear stress is an important factor for remodeling adhesion, morphology, and function of ECs both in vivo and in vitro [72]. Compared with static culture, dynamic culture is helpful to improve cell proliferation on vascular grafts, which is more beneficial for extracellular matrix deposition and anti-thrombogenesis, as well as reducing the inflammatory response of vascular grafts [73]. Furthermore, the pretreatment with shear stress enhances the subsequent retention of ECs after implantation in vivo [74]. Herein, a perfusion system was used to further estimate the adhesion and proliferation of ECs under flow shear stress (Fig. 7B). As shown in Fig. 7C, the numbers of HUVECs on PCL and PCL/Cu mats had no significant difference under static conditions for 6 h. However, under the stress of flow shear, only a few cells adhered on the inner wall of PCL grafts. In contrast, there were still many HUVECs on the inner wall of PCL/Cu grafts. It was due to the PCL/Cu layer's superior hydrophilicity, which encouraged HUVEC adhesion.

To further evaluate the proliferation of HUVECs, the grafts were perfused for 5 d. It was observed with SEM that a few round HUVECs were attached to the PCL grafts, indicating poor cytocompatibility (Fig. 7D). In comparison, the entire intima of bilayer grafts was covered with densely packed HUVECs, and nearly no fibers were observed. HUVECs adhered together and formed an endothelium layer. The cell viability with CCK-8 assay also illustrated that the proliferation of HUVECs on bilayer grafts was faster than that on PCL grafts under flow shear stress (Fig. 7E). These results suggested that bilayer grafts possess the potential to promote the formation of the endothelial layer and accelerate vascular remodeling under blood flow.

2.10. Vascular graft implantation and patency evaluation

PLCL/KAT-PCL/Cu grafts were tested in rat abdominal aorta replacement models. As depicted in Fig. 8A, the diameter of the transplanted artificial vascular grafts was consistent with the autologous abdominal aorta of the rat. After restoring blood flow, there was no bleeding at the vascular anastomosis. The autologous blood vessel and H_2S/NO artificial blood vessel were filled, and the blood vessels pulsated normally. The images of the color Doppler-ultrasonic imaging suggested that the PLCL/KAT-PCL/Cu grafts remained 100% patency with clear

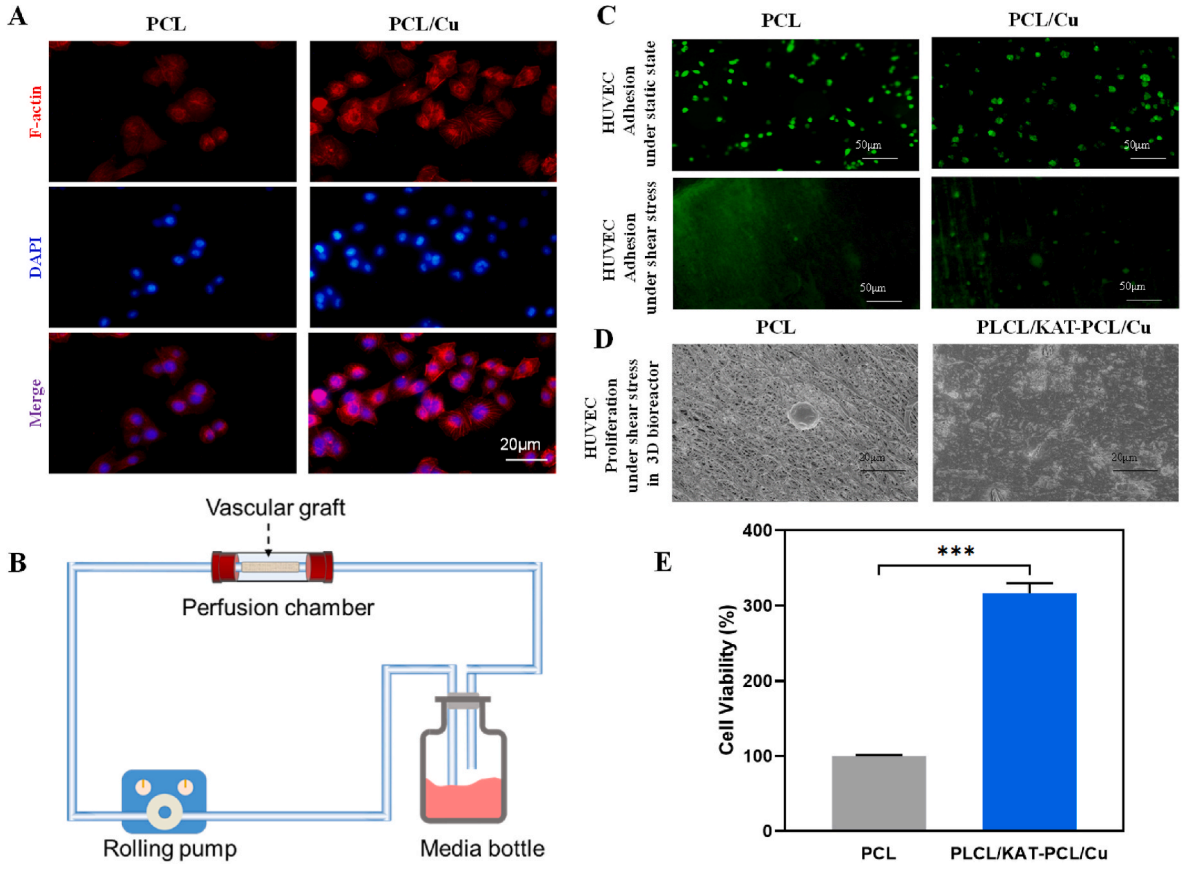

Fig. 7. (A) Immunofluorescent staining images of HUVEC with F-actin (red) and DAPI(blue) on PCL and PCL/Cu in the presence of GSNO(50 μM) after 1 d of culture; (B) Perfusion circuit system for 3D-perfusion culture; (C) Fluorescence images of adhesion and growth of HUVEC on PCL and PCL/Cu under static state and shear stress state in a 3D perfusion bioreactor for 6 h; (D) SEM of adhesion and growth of HUVEC on PCL and PCL/Cu under flow shear stress in a 3D perfusion bioreactor for 5 d; (E) Viability of HUVECs on PCL and bilayer PLCL/KAT-PCL/Cu grafts (*** indicates the significant differences between groups at $p < 0.001$).

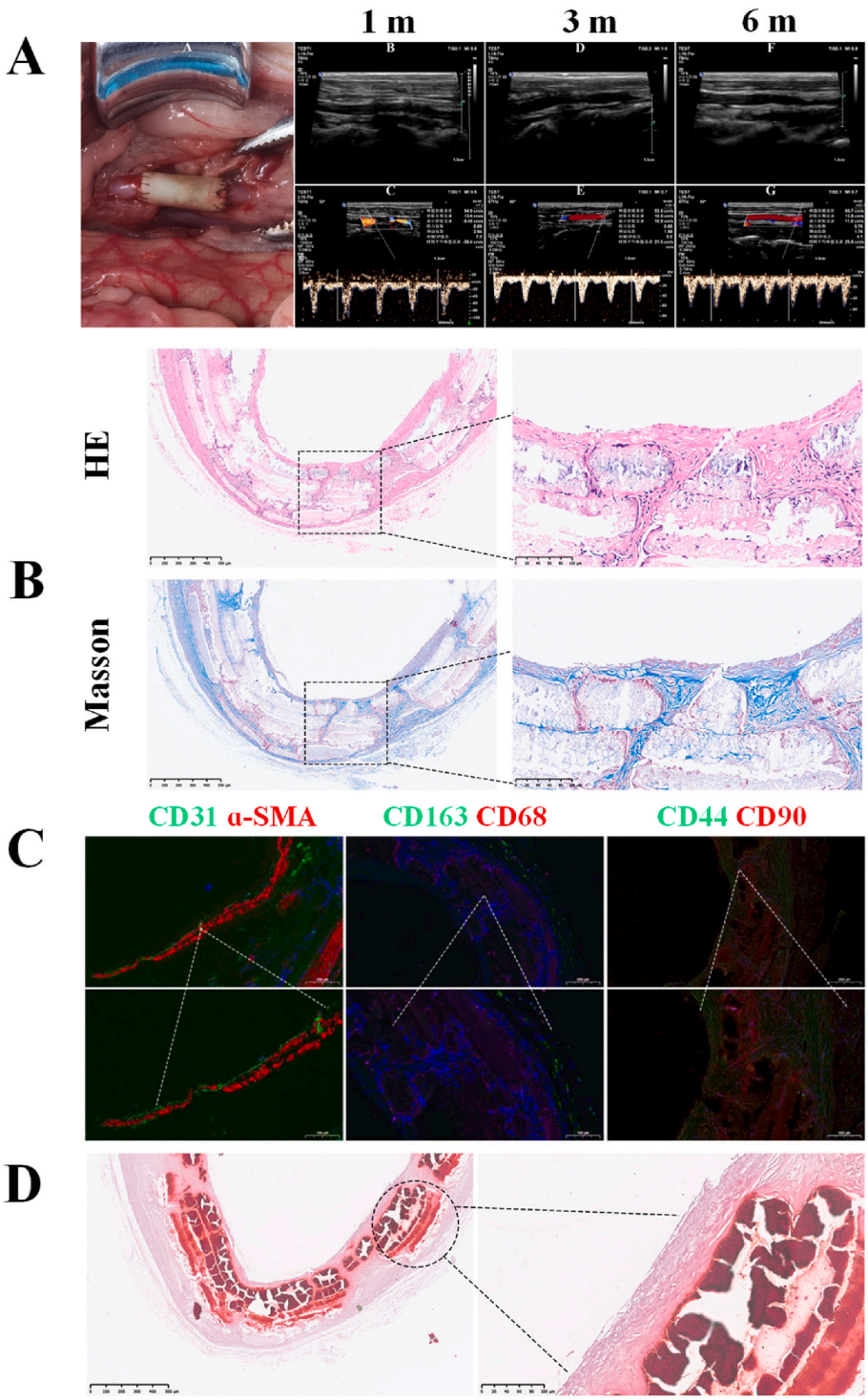

Fig. 8. (A) Re-establishment of the rat carotid artery with grafts, and Doppler-ultrasonic images of PLCL/KAT-PCL/Cu grafts at 1 month (1 m), 3 months (3 m), and 6 months (6 m) after surgery, respectively; (B) HE and Masson staining of cross-sections of PLCL/KAT-PCL/Cu grafts after implantation for 6 months (scale bar = 100 μm); (C) Immunofluorescence staining micrographs of CD31, α-SMA, CD163, CD68, CD44, and CD90 from cross-sections of PLCL/KAT-PCL/Cu grafts after implantation for 6 months (upper line, scale bar = 200 μm; lower line, scale bar = 100 μm); (D) Alizarin red staining on the sections of grafts, and calcification deposits were stained dark red (scale bar in left = 500 μm, scale bar in right = 100 μm).

flow signals after surgery for 6 months (Fig. 8A). More importantly, no dilatation of the lumen occurred during the follow-up period, indicating that the PLCL/KAT-PCL/Cu grafts possessed good mechanical stability and could greatly withstand the abdominal aorta blood pressure in rats.

Histological staining (H&E staining and Masson staining) was conducted to describe the ECM deposition in the explanted vascular grafts. As shown in Fig. 8B, H&E staining revealed that the PLCL/KAT-PCL/Cu grafts remained patency without thrombosis after implantation for 6 months, similar to the autologous abdominal aorta. The inner diameter of the grafts was not decreased, and the neointima was well regenerated without hyperplasia. It was attributed to the dual regulation of NO/H_2S, which promoted the proliferation and migration of HUVECs and inhibited the excessive proliferation of HUASMCs, resulting in long-term patency. It was worth mentioning that the PLCL/KAT-PCL/Cu grafts contained abundant bundles of collagen fibers from Masson staining. Furthermore, the degradation rate of PLCL/KAT-PCL/Cu grafts achieved a good match with the rate of tissue regeneration after 6 months of implantation, ensuring that the grafts had sufficient mechanical properties without aneurysm dilation.

Rapid and complete endothelialization is pivotal to long-term patency. The components of the neointima were further analyzed by immunofluorescence. The continuous endothelium and smooth muscle

layer gradually formed on the PLCL/KAT-PCL/Cu grafts at 6 months after surgery on immunofluorescence staining images of CD31 (red, endothelial cell-specific marker) and α-SMA (green, smooth muscle cell-specific marker), suggesting complete endothelialization (Fig. 8C). Due to the effect of H_2S, the thickness of the smooth muscle layer in the neointima was moderate, and there was no excessive hyperplasia. In the regenerated vascular tissue, macrophages of type M2 (anti-inflammatory type) were dominant, indicating that the inflammatory response had basically disappeared and tissue regeneration was well established. Mesenchymal stem cells (MSCs) can be differentiated into vascular endothelial cells to increase the elasticity and vascular permeability of blood vessels, thereby improving vascular microcirculation. MSCs were labeled by CD44 and CD90, and the presence of resident MSCs in the regenerated vascular tissues indicated that the vascular regeneration process was complete and retained the potential for rapid revascularization.

Arterial calcification increases stiffness and affects the compliance of grafts. Severe arterial calcification can lead to heart failure, atherosclerotic plaque rupture, and myocardial infarction [75]. SDVGs, especially those derived from the acellular matrix, often have low patency rates due to vascular calcification. Therefore, the potential of vascular grafts to prevent calcification is indispensable for the reconstruction of diseased vessels. After implantation for 6 months, the sections of PLCL/KAT-PCL/Cu grafts were stained with alizarin red solution for calcification analysis (Fig. 8D). There was nearly no calcium deposition occurring in the inner layer of grafts, the outer layer of grafts, and the interval regenerated tissues of the degraded grafts. However, calcification was found only on the non-degraded section of the grafts. In this respect, it was predicted that the PLCL/KAT-PCL/Cu grafts would fully achieve autologous vascular regeneration without vascular calcification after the grafts were completely degraded. These results were consistent with the hypothesis that the fast-degrading grafts would inhibit calcification [76]. High phosphorus, high glucose, and abnormal lipid metabolism cause an oxidative stress response that transforms HUASMCs into an osteogenic-like phenotype, leading to the development of vascular calcification [77,78]. Growing evidence proved that H_2S possesses anti-arterial calcification effects by inhibiting Pit-1 on HUASMCs membrane to inhibit phosphate absorption, scavenging oxidative stress, and inhibiting the up-regulation of osteoblast-specific genes [79]. H_2S was also found to inhibit the calcification and osteoblastic differentiation of vascular smooth muscle cells [80]. All of these properties contributed to the reduction in calcification. These results demonstrated that the bilayer grafts could effectively alleviate arterial calcification and prevent vascular stenosis. Although the mechanism of calcification is not fully understood, improved biocompatibility and reduced inflammation are widely recognized to be beneficial to anti-calcification.

Atherosclerosis is a chronic vascular inflammatory disease that is related to endothelial cell injury and macrophage infiltration [81,82]. Inhibitions of vascular inflammation and alleviation of endothelial dysfunction are helpful to reduce the incidence of cardiovascular diseases such as atherosclerosis. H_2S and NO have inflammatory inhibitory effects by inhibiting the activation of the NF-κB pathway, reducing pro-inflammatory factor release, inhibiting oxidative stress, and reducing lipid peroxidation [83–85]. To further test the inflammatory stimulation of tissues during the degradation of grafts, WB analysis was performed (Fig. 9). Obviously, the expressions of IL-4 and IL10 (anti--inflammatory factors) were significantly higher than those of IL-6 and IL-1β(pro-inflammatory factors), proving that the PLCL/KAT-PCL/Cu grafts did not cause an inflammatory reaction during degradation due to the release of dual gases. The releases of NO and H_2S are capable of reducing inflammation synergistically.

3. Conclusions

To summarize, bilayer vascular grafts with the capability for NO and H_2S dual release were designed and developed. The PCL/Cu inner layer was capable to generate NO, thereby accelerating the growth and migration of HUVECs. The PLCL/KAT outer layer inhibited the proliferation and migration of HUASMCs due to the prolonged release of H_2S. Dual releases of NO and H_2S gasotransmitters could enhance their respective production, resulting in enhanced promotion of HUVECs and inhibition of HUASMCs owing to their combined actions. The grafts displayed better selectivity for HUVECs and promoted the formation of the EC layer under flow shear stress. In a rat abdominal aorta replacement model, the grafts remained patency without calcification for 6 months. More importantly, these grafts were able to facilitate rapid endothelialization and alleviate neointimal hyperplasia without obvious injury, inflammation, or thrombosis. Taken together, NO and H_2S dual-releasing bi-layer grafts will be a greatly promising candidate for small-diameter vascular grafts with rapid endothelialization and promoting vascular remolding.

4. Experimental section

4.1. Materials

Poly (ε-caprolactone) (PCL, MW 80,000) and poly (L-lactide-co-caprolactone) (PLCL, MW 80,000) were purchased from Daigang Biomaterial Co. Ltd. (Jinan, China). Ethylenediamine tetraacetic acid disodium salt, ethylenediamine, sodium chloroacetate, and cupric sulfate were purchased from Sinopharm Chemical Reagent Co. Ltd. (Shanghai, China). The circular metal rod (Φ 2 mm) was used as a collector for electrospinning tubular grafts. All other chemicals were

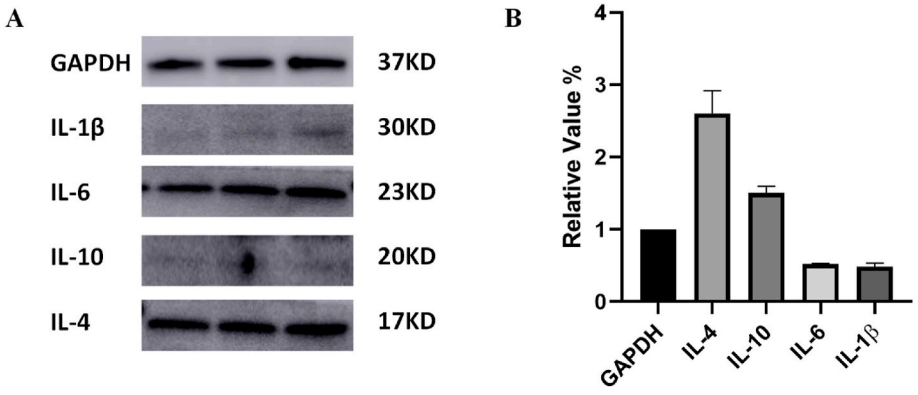

Fig. 9. (A) Representative Western blot (WB) gel depicts the protein expression of GAPDH, IL-4, IL-10, 1L-6, and IL-1β after implantation for 6 months (Upper); (B) Quantitative protein expression analysis of GAPDH, IL-4, IL-10, 1L-6, and IL-1β after implantation for 6 months (Lower). Using GAPDH as a loading control, the protein expression was normalized in each case.

analytical grade and used without further purification.

4.2. Preparation of keratin-based hydrogen sulfide donor

Keratin-based hydrogen sulfide donor was synthesized according to previous literature [86]. 4-Aminobenzothioamide was synthesized as described previously [87]. Keratin was extracted from human hair, and modified with iodoacetic acid in our lab [88]. 4-Aminobenzothioamide was conjugated with keratin via carbodiimide/N-hydroxysuccinimide (EDC/NHS) chemistry and keratin-aminobenzothioamide conjugate (denoted as KAT) was obtained as a biomacromolecular H_2S donor.

4.3. Fabrication of PCL/cu mats as the inner layer

PCL mats were first prepared by electrospinning. PCL was dissolved in hexafluoroisopropanol (HFIP) to a total concentration of 8 wt% and then transferred to a metal syringe (23G) connected to a high-voltage power supply. The feed rate, voltage, and collected distance were adjusted to 1.0 mL/h, 20 kV, and 15 cm, respectively. A cylindrical collector with a diameter of 20 cm and a rotating speed of 12 rpm was used to prepare the PCL layer.

The PCL layer was immersed in an ethylenediamine solution (40%) at 37 °C for a predetermined time and washed with deionized water. Then, the layer was immersed in a mixture of iodoacetic acid and sodium hydroxide (NaOH) solution for 8 h. Afterward, the mats were placed in 0.5 M $CuSO_4$ solution for 1 h to immobilize the Cu(II) ions and then washed with deionized water. The density of aminos was tested by ninhydrin and described in Fig. 9.

4.4. Fabrication of PLCL/KAT mats as the outer layer

The outer layer of PLCL/KAT mats was fabricated with coaxial electrospinning. In detail, KAT was dissolved in water with a concentration of 30 mg/mL for the core solution, and PLCL was dissolved in HFIP at a concentration of 8 wt% for the shell solution. The inside diameters of the inner needle and outer needle were 0.4 mm and 1 mm, respectively. The coaxial needle was directly connected to a high-voltage power supply and the voltage was set to 20 kV. The core solution was injected at a flow rate of 0.5 mL/h, while the shell solution (PLCL) was injected at a flow rate of 1.5 mL/h. The mats were collected on the cylindrical collector with a diameter of 20 cm and a rotating speed of 12 rpm. All the samples were dried in a vacuum at room temperature for 6 h for further research.

4.5. Fabrication of tubular bilayer grafts

PCL/Cu inner layer was first prepared and the PLCL/KAT layer was fabricated by sequential electrospinning. Briefly, the needle was fixed on a stepping motor to ensure the reciprocating motion with a constant speed. A round metal rod with a 2 mm diameter was used to fabricate tubular grafts at 1200 rpm/min. All the as-spun samples were dried in a vacuum at room temperature for 6 h to remove residual solvent.

4.6. Catalytic generation of NO with the inner layer in vitro

The PCL and PCL/Cu mats (50 mg) were immersed in GSNO solution (2 mL, 50 μM in PBS) and incubated at 37 °C, respectively. 50 μL of the sustained-release solution was collected and replaced with the same volume of GSNO solution each time. The amount of NO was tested using Griess reagent.

To evaluate the stability of the fixed copper (II) ions, PCL/Cu mats were immersed in 50 μM EDTA for 30 min and then washed with deionized water, and the cumulative release profile of NO was tested.

4.7. Release of H_2S with the outer layer in vitro

The H_2S release profile of PLCL/KAT was tested by methylene blue method [89]. PLCL mats (50 mg) and PLCL/KAT mats (50 mg) were immersed in 1 mL of GSH solution in PBS(1 mM, pH 7.4), respectively. At a pre-determined interval, the solution was collected and replenished with a fresh working solution. The collected solution was reacted with 100 μL zinc acetate (1% w/v in H_2O) for 30 min and centrifuged at 12, 000 rpm for 10 min. The supernatant was discarded and then added with PBS (600 μL), N,N-dimethyl-1,4-phenylenediamine sulfate (20 mM, 100 μL), and $FeCl_3$ (30 mM, 100 μL). The optical density (OD) value at 670 nm was measured by a microplate reader (BioTek ELx800, USA) after 30 min.

4.8. The effect of NO release on the proliferation of HUVECs and HUASMCs

The effect of NO release on the proliferation of HUVECs was evaluated by the MTT assay. In brief, PCL and PCL/Cu mats were cut into circular slices (Φ 1.4 cm) and put in 24-well plates, respectively. HUVECs were seeded at a density of 1×10^4 cells/mL each and incubated for 72 h with 5% CO_2 at 37 °C. For the NO-generated group, GSNO was added with a final concentration of 50 μM and replenished every 12 h. The media was replaced with fresh media and then the MTT solution (5 mg/mL, 50 μL) was added to each well. After incubation for another 4 h, the media was discarded and DMSO was added to dissolve the converted formazan. Then, 100 μL solution was transferred into 96-well plates and the OD values were measured using a microplate reader (BioTek ELx800, USA) at 490 nm.

The effect of NO release on HUASMCs proliferation was conducted similarly to that on HUVECs.

4.9. The effect of H_2S release on the proliferation of HUVECs and HUASMCs

The effect of H_2S release on the proliferation of HUVECs was evaluated by the MTT assay. In brief, PLCL and PLCL/KAT mats were cut into circular slices with a diameter of 1.4 cm and put in 24-well plates, respectively. HUVECs were seeded on the mats at a density of 1×10^4 cells/mL per well and incubated for 72 h with 5% CO_2 at 37 °C. For PLCL/KAT groups, GSH was added with a final concentration of 50 μM and replenished every 12 h. The media was replaced with fresh media before the MTT was added. After incubation for another 4 h, the media was discarded and DMSO was added to dissolve the converted formazan. Then, 100 μL solution was transferred into 96-well plates and the OD values were measured using a microplate reader (BioTek ELx800, USA) at 490 nm.

The effect of H_2S release on HUASMCs proliferation was conducted similarly to that on HUVECs.

4.10. The effect of NO and H_2S dual release on the migration of HUVECs and HUASMCs

The PCL and PCL/Cu mats were cut into rectangle pieces of 25 mm × 15 mm and placed in a 6-well culture plate for the migration test of HUVECs. A stainless steel bar (1 mm × 1 mm × 10 mm) was added to cover each piece. HUVECs were stained via Cell Tracker green CMFDA dye (1.5×10^{-5} M) for 1 h then detached by trypsin and seeded at a density of 5×10^5 cells/mL. GSNO was added with a final concentration of 50 μM for NO-generated groups. After incubation for 4 h, the stainless steel bars were removed and the initial position was recorded by a fluorescent microscope (MSHOT MF53, China). The final state was recorded and the migrated distance was measured by Image J after 24 h of incubation.

HUASMCs were stained via Cell Tracker green CMFDA dye (1.5×10^{-5} M) for 1 h after cells reached 80% confluence and seeded on PLCL

and PLCL/KATs, respectively. The migration was performed similarly to that of the HUVECs test. GSH was added with a final concentration of 200 μM for H_2S-generated groups.

4.11. Co-culture of HUVECs and HUASMCs

CellTracker red CMTPX dye (1.5×10^{-5} M) and CellTracker Green CMFDA dye (1.5×10^{-5} M) in serum-free medium were separately added into to HUVECs and HUASMCs for 1 h. After washing with PBS and detaching with trypsin, the cells were diluted to 3×10^4 cells/mL and mixed with a volume ratio of 1:1. A total of 1 mL cell suspension was seeded into each well with PLCL/KAT-PCL/Cu mats and incubated for 24 h under 5% CO_2 at 37 °C. The competitive proliferation was observed using a fluorescence microscope (MSHOT MF53, China). GSNO was added with a final concentration of 50 μM for NO-generated groups and GSH was added with a final concentration of 200 μM for H_2S-generated groups. The number of HUVECs and HUASMCs was counted from four pictures by ImageJ software.

4.12. Immunofluorescent staining for F-actin of HUVECs

HUVECs were digested with 0.25% trypsin and diluted with RPMI-1640 medium (20% fetal bovine serum, 50 μM GSNO) to obtain cell suspension with a density of 2×10^4 cells/mL. The suspension was seeded in a 24-well plate, and PCL and PCL/Cu slices with a diameter of 14 mm were added to the well, respectively. After incubation for 24 h under a 5% CO_2 atmosphere at 37 °C, the media was discarded and the plate was washed with PBS. HUVECs were fixed in 1% glutaraldehyde solution at room temperature for 20 min, then washed with PBS containing 0.1% Triton X-100 three times. The cells were dyed with Actin-Tracker Red for 1 h in the dark and then washed with PBS containing 0.1% Triton X-100 five times. The DAPI was added to each well to dye the nucleus for 5 min. The cells were observed and recorded using a fluorescence microscope (MSHOT MF53, China).

4.13. Synergistic effects of dual NO and H_2S

4.13.1. Effect of H_2S release on NO secretion of HUVECs

HUVECs were seeded in a 60 mm cell culture dish. After the cells were expanded to 80%, the medium was replaced with 3 mL RCMI-1640 medium (20% fetal bovine serum, 1% double antibody, 200 μM GSH). PLCL and PLCL/KAT mats (2 cm × 4 cm) were added and incubated at 37 °C for 72 h. GSH was added every 24 h to maintain the constant concentration. At certain intervals, 50 μL supernatant from each dish was transferred into 96-well blended with 100 μL Greiss agent in the dark for 15 min. The NO concentration was tested at 540 nm with a microplate reader (BioTek ELx800, USA).

4.13.2. Effect of NO release on H_2S secretion of HUASMCs

HUASMCs were seeded in a 60 mm cell culture dish. After the cells were expanded to 80%, GSNO was added to the final concentration of 50 μM. PCL/Cu mats (2 cm × 4 cm) were added and incubated at 37 °C for 72 h. The supernatant was taken out and replenished with an equal volume of fresh media containing 50 μM GSNO. The collection media was reacted with 100 μL zinc acetate (1% w/v in H_2O) for 30 min and centrifuged at 12,000 rpm. The H_2S concentration was measured by the methylene blue method.

4.13.3. The proliferation of HUVECs and HUASMCs

In brief, PLCL and PLCL/KAT mats were cut into circular slices with a diameter of 1.4 cm and put in a 24-well plate. HUVECs suspension (10^4 cells/mL, 1 mL) was seeded in each well and incubated with 5% CO_2 at 37 °C for 48 h. For PCL/HAT groups, GSH was added with a final concentration of 200 μM and replenished per 12 h. The media was replaced with fresh media before the MTT was added. After incubation for another 4 h, the media was discarded, and 500 μL DMSO was added to dissolve the converted formazan. Then, 100 μL solution was transferred into a 96-well plate and the OD values were measured using a microplate reader (BioTek ELx800, USA) at 490 nm.

The proliferation of HUASMCs on PCL/Cu mats in the presence of GSNO(50 μM) was conducted similarly to that of HUVECs.

4.14. 3D-perfusion culture

A homemade perfusion circuit system consisting of a perfusion chamber, a rolling pump, and a media bottle was used to estimate graft endothelialization under flow shear stress in vitro. The grafts were treated with ultraviolet radiation for 30 min and incubated in PBS containing 1% penicillin G–streptomycin for sterilization. HUVECs with a density of 4×10^4 cells/mL were added to the medium reservoir. Then, the grafts were placed in the chamber and exposed to a flow rate of 20 mL/min in an incubator at 37 °C under 5% CO_2. At predetermined times, the grafts were removed to estimate the adhesion and proliferation of HUVECs by fluorescent microscope and SEM. The cell viability of HUVEC was tested by CCK-8 kit after 5 days of incubation.

4.15. In vivo implantation

The tubular grafts (inner diameter = 2.0 mm) with inner layer thickness of ca. 100 μm and outer layer thickness of ca. 250 μm were fabricated and sterilized. The tubular grafts (length = 1 cm) were implanted into the abdominal arteries of rats following a previously reported protocol. Twelve 8-week-old male SD rats were purchased from Cowen's Biotechnology Co., LTD. (Shanghai, China). All procedures were conducted following the ARRIVE Guide and have been approved by the Animal Ethics Committee of Shanghai Children's Medical Center (SCMC), Shanghai Jiao Tong University School of Medicine. Experiments were conducted in strict accordance with the Guidelines for the care and use of laboratory animals established by the National Institutes of Health (NIH publication N01-OD-4-2139, Rev.2). Briefly, rats were anesthetized by inhalation with mixed isoflurane at 3% and maintained 1.5%, respectively. A midline skin incision was made and the rat intestines were pushed aside to expose the infrarenal aorta. After the administration of 300 IU/kg heparin, the abdominal aorta was separated and blocked with two vascular clips, then the abdominal aorta was excised and the defect was established. The grafts were as implanted with 9–0 sutures (Ethicon, Shanghai, China) by end-to-end continuous sutures. After re-establishing blood flow, the abdominal cavity and the skin were closed. Doppler sonography was used to evaluate the vascular function after implantation of 1, 3, and 6 months. Furthermore, the velocity of blood flow in the vascular grafts was quantified by Doppler waveform analysis.

After 6 months of implantation, the entire graft-containing tissue was harvested from euthanized rats to assess endothelialization. Four graft specimens were cut lengthwise for Western blot (WB) assay. The other eight specimens of vascular grafts were stained with H&E staining, Masson trichromatic staining, immunofluorescence staining, and alizarin red staining. To accurately assess tissue regeneration, all specimens were stained from the middle part of the vascular grafts. For in vivo calcification analysis, the sections of graft specimens were stained with alizarin red dye.

Data availability

The data that support the findings of this study are available from the corresponding author upon reasonable request.

CRediT authorship contribution statement

Pengfei Li: Writing – original draft, performed the experiments. **Fubang Liang:** Writing – original draft, performed the experiments. **Lijuan Wang:** Writing – original draft, performed the experiments.

Dawei Jin: Validation. **Yushuang Shang:** Validation. **Xu Liu:** Validation. **Yanjun Pan:** Validation. **Jiang Yuan:** Funding acquisition, Writing – review & editing. **Jian Shen:** Funding acquisition, Writing – review & editing. **Meng Yin:** Funding acquisition, Writing – review & editing.

Declaration of competing interest

We declare that we do not have any commercial or associative interest that represents a conflict of interest in connection with the work submitted.

PENGFEI LI, FUBANG LIANG, LIJUAN WANG, DAWEI JIN, YUSHUANG SHANG, XU LIU, YANJUN PAN, JIANG YUAN, JIAN SHEN, MENG YIN.

Acknowledgements

This work was supported by the National Natural Science Fund of China(81873923), Jiangsu Higher Education Institutions(19KJA310001 and PAPD), and Jiangsu Collaborative Innovation Center of Biomedical Functional Materials.

Appendix A. Supplementary data

Supplementary data to this article can be found online at https://doi.org/10.1016/j.bioactmat.2023.07.020.

References

[1] D.P. Taggart, Current status of arterial grafts for coronary artery bypass grafting, Ann. Cardiothorac. Surg. 2 (2013) 427–430.
[2] M.R. de Vries, K.H. Simons, J.W. Jukema, J. Braun, P.H. Quax, Vein graft failure: from pathophysiology to clinical outcomes, Nat. Rev. Cardiol. 13 (2016) 451–470.
[3] M. Lopera Higuita, J.F. Lopera Giraldo, T.L. Sarrafian, L.G. Griffiths, Tissue engineered bovine saphenous vein extracellular matrix scaffolds produced via antigen removal achieve high in vivo patency rates, Acta Biomater. 134 (2021) 144–159.
[4] W. Gong, D. Lei, S. Li, P. Huang, Q. Qi, Y. Sun, Y. Zhang, Z. Wang, Z. You, X. Ye, Q. Zhao, Hybrid small-diameter vascular grafts: anti-expansion effect of electrospun poly ε-caprolactone on heparin-coated decellularized matrices, Biomaterials 76 (2016) 359–370.
[5] Y. Yang, D. Lei, H. Zou, S. Huang, Q. Yang, S. Li, F. Qing, X. Ye, Z. You, Q. Zhao, Hybrid electrospun rapamycin-loaded small-diameter decellularized vascular grafts effectively inhibit intimal hyperplasia, Acta Biomater. 97 (2019) 321–332.
[6] A. de Mel, G. Jell, M.M. Stevens, A.M. Seifalian, Biofunctionalization of biomaterials for accelerated in situ endothelialization: a review, Biomacromolecules 9 (2008) 2969–2979.
[7] J. Zhao, Y. Feng, Surface engineering of cardiovascular devices for improved hemocompatibility and rapid endothelialization, Adv Healthc Mater 9 (2020), 2000920.
[8] M. Kushwaha, J.M. Anderson, C.A. Bosworth, A. Andukuri, W.P. Minor, J. R. Lancaster, P.G. Anderson, B.C. Brott, H. Jun, A nitric oxide releasing, self-assembled peptide amphiphile matrix that mimics native endothelium for coating implantable cardiovascular devices, Biomaterials 31 (2010) 1502–1508.
[9] F. Otsuka, A.V. Finn, S.K. Yazdani, M. Nakano, F.D. Kolodgie, R. Virmani, The importance of the endothelium in atherothrombosis and coronary stenting, Nat. Rev. Cardiol. 9 (2012) 439–453.
[10] N. Naghavi, A. de Mel, O.S. Alavijeh, B.G. Cousins, A.M. Seifalian, Nitric oxide donors for cardiovascular implant applications, Small 9 (2013) 22–35.
[11] J.Y. Jeremy, D. Rowe, A.M. Emsley, A.C. Newby, Nitric oxide and the proliferation of vascular smooth muscle cells, Cardiovasc. Res. 43 (1999) 580–594.
[12] A.W. Carpenter, M.H. Schoenfisch, Nitric oxide release: Part II. Therapeutic applications, Chem. Soc. Rev. 41 (2012) 3742–3752.
[13] F. Kabirian, P.B. Milan, A. Zamanian, R. Heying, M. Mozafari, Nitric oxide-releasing vascular grafts: a therapeutic strategy to promote angiogenic activity and endothelium regeneration, Acta Biomater. 92 (2019) 82–91.
[14] K.S. Bohl, J.L. West, Nitric oxide-generating polymers reduce platelet adhesion and smooth muscle cell proliferation, Biomaterials 21 (2000) 2273–2278.
[15] P. Li, D. Jin, J. Dou, L. Wang, Y. Wang, X. Jin, X. Han, I.K. Kang, J. Yuan, J. Shen, M. Yin, Nitric oxide-releasing poly(ε-caprolactone)/S-nitrosylated keratin biocomposite scaffolds for potential small-diameter vascular grafts, Int. J. Biol. Macromol. 189 (2021) 516–527.
[16] P.G. Wang, M. Xian, X. Tang, X. Wu, Z. Wen, T. Cai, A.J. Janczuk, Nitric oxide donors: chemical activities and biological applications, Chem. Rev. 102 (2002) 1091–1134.
[17] J. Mendhi, I. Prasadam, S. Subramaniam, L. Bai, W. Gao, J. Batra, R. Crawford, Y. Yang, Y. Xiao, Nitric oxide generating coating alters hematoma structure and soft tissue healing, Appl. Mater. Today 22 (2021), 100919.
[18] C.W. McCarthy, R.J. Guillory II, J. Goldman, M.C. Frost, Transition-metal-mediated release of nitric oxide (NO) from S-nitroso-N-acetyl-d-penicillamine (SNAP): potential applications for endogenous release of NO at the surface of stents via corrosion products, ACS Appl. Mater. Interfaces 8 (2016) 10128–10135.
[19] X.Y. Zhang, Y.B. Wang, J. Liu, J. Shi, D. Mao, A.C. Midgley, X.G. Leng, D.L. Kong, Z. H. Wang, B. Liu, S.F. Wang, A metal-organic-framework incorporated vascular graft for sustained nitric oxide generation and long-term vascular patency, Chem. Eng. J. 421 (2021), 129577.
[20] C. Miao, J. Du, J. Dou, C. Wang, L. Wang, J. Yuan, J. Shen, M. Yin, Facile fabrication of copper incorporated poly(ε-caprolactone)/keratin mats for tissue-engineered vascular grafts with the potential of catalytic nitric oxide generation, J. Mater. Chem. B 10 (2022) 6158–6170.
[21] A. Martelli, L. Testai, A. Marino, M.C. Breschi, F. Da Settimo, V. Calderone, Hydrogen sulphide: biopharmacological roles in the cardiovascular system and pharmaceutical perspectives, Curr. Med. Chem. 19 (2012) 3325–3336.
[22] M.J. Wang, W.J. Cai, Y.C. Zhu, Hydrogen sulphide in cardiovascular system: a cascade from interaction between sulphur atoms and signalling molecules, Life Sci. 153 (2016) 188–197.
[23] L. Li, P. Rose, P.K. Moore, Hydrogen sulfide and cell signaling, Annu. Rev. Pharmacol. Toxicol. 51 (2011) 169–187.
[24] M.L. Lo Faro, B. Fox, J.L. Whatmore, P.G. Winyard, M. Whiteman, Hydrogen sulfide and nitric oxide interactions in inflammation, Nitric Oxide 41 (2014) 38–47.
[25] C. Szabó, Hydrogen sulfide and its therapeutic potential, Nat. Rev. Drug Discov. 6 (2007) 917–935.
[26] A.S. Zhao, D. Zou, H.H. Wang, X. Han, P. Yang, N. Huang, Hydrogen sulphide-releasing aspirin enhances cell capabilities of anti-oxidative lesions and anti-inflammation, Med. Gas Res. 9 (2019) 145–152.
[27] A. Longchamp, K. Kaur, D. Macabrey, C. Dubuis, J.M. Corpataux, S. Deglise, J. B. Matson, F. Allagnat, Hydrogen sulfide-releasing peptide hydrogel limits the development of intimal hyperplasia in human vein segments, Acta Biomater. 97 (2019) 374–384.
[28] A. Papapetropoulos, A. Pyriochou, Z. Altaany, G. Yang, A. Marazioti, Z. Zhou, M. G. Jeschke, L.K. Branski, D.N. Herndon, R. Wang, C. Szabó, Hydrogen sulfide is an endogenous stimulator of angiogenesis, Proc. Natl. Acad. Sci. U.S.A. 106 (2009) 21972–21977.
[29] Q. Li, J.R. Lancaster, Chemical foundations of hydrogen sulfide biology, Nitric Oxide 35 (2013) 21–34.
[30] C. Coletta, A. Papapetropoulos, K. Erdelyi, G. Olah, K. Modis, P. Panopoulos, A. Asimakopoulou, D. Gero, I. Sharina, E. Martin, C. Szabo, Hydrogen sulfide and nitric oxide are mutually dependent in the regulation of angiogenesis and endothelium-dependent vasorelaxation, Proc. Natl. Acad. Sci. U.S.A. 109 (2012) 9161–9166.
[31] R. Hosoki, N. Matsuki, H. Kimura, The possible role of hydrogen sulfide as an endogenous smooth muscle relaxant in synergy with nitric oxide, Biochem. Biophys. Res. Commun. 237 (1997) 527–531.
[32] W. Zhao, R. Wang, H_2S-induced vasorelaxation and underlying cellular and molecular mechanisms, Am. J. Physiol. Heart Circ. Physiol. 283 (2002) H474–H480.
[33] J. Lee, C. Yang, S. Ahn, Y. Choi, K. Lee, Enhanced NO-induced angiogenesis via NO/H_2S co-delivery from self-assembled nanoparticles, Biomater. Sci. 9 (2021) 5150–5159.
[34] Q.C. Yong, J.L. Cheong, F. Hua, L.W. Deng, Y.M. Khoo, H.S. Lee, A. Perry, M. Wood, M. Whiteman, J.S. Bian, Regulation of heart function by endogenous gaseous mediators-crosstalk between nitric oxide and hydrogen sulfide, Antioxidants Redox Signal. 14 (2011) 2081–2091.
[35] D. Wu, Q.X. Hu, D.Q. Zhu, An Update on Hydrogen Sulfide and Nitric Oxide Interactions in the Cardiovascular System, Oxid Med Cell Longev, 2018, 4579140.
[36] C.M. Vaz, S. van Tuijl, C.V.C. Bouten, F.P.T. Baaijens, Design of scaffolds for blood vessel tissue engineering using a multi-layering electrospinning technique, Acta Biomater. 1 (2005) 575–582.
[37] L. Ye, J. Cao, L. Chen, X. Geng, A. Zhang, L. Guo, Y. Gu, Z. Feng, The fabrication of double layer tubular vascular tissue engineering scaffold via coaxial electrospinning and its 3D cell coculture, J. Biomed. Mater. Res. 103 (2015) 3863–3871.
[38] W.Z. Wang, W. Nie, X.J. Zhou, W. Feng, L. Chen, Q.Q. Zhang, Z.W. You, Q.S. Shi, C. Peng, C.L. He, Fabrication of heterogeneous porous bilayered nanofibrous vascular grafts by two-step phase separation technique, Acta Biomater. 79 (2018) 168–181.
[39] T. Wu, J.L. Zhang, Y.F. Wang, B.B. Sun, M. Yin, G.L. Bowlin, X.M. Mo, Design and fabrication of a biomimetic vascular scaffold promoting in situ endothelialization and tunica media regeneration, ACS Appl. Bio Mater. 1 (2018) 833–844.
[40] C. Cui, M.L. Wen, F. Zhou, Y.H. Zhao, X.Y. Yuan, Target regulation of both VECs and VSMCs by dual-loading miRNA-126 and miRNA-145 in the bilayered electrospun membrane for small-diameter vascular regeneration, J. Biomed. Mater. Res. 107 (2019) 371–382.
[41] W. He, A. Nieponice, L. Soletti, Y. Hong, B. Gharaibeh, M. Crisan, A. Usas, B. Peault, J. Huard, W.R. Wagner, D.A. Vorp, Pericyte-based human tissue engineered vascular grafts, Biomaterials 31 (2010) 8235–8244.
[42] X.R. Guo, J.J. Zhu, H.M. Zhang, Z.W. You, Y. Morsi, X.M. Mo, T.H. Zhu, Facile preparation of a controlled-release tubular scaffold for blood vessel implantation, J. Colloid Interface Sci. 539 (2019) 351–360.

[43] C.L. Zhang, Q. Xie, R.T. Cha, L. Ding, L.J. Jia, L. Mou, S.Y. Cheng, N.X. Wang, Z. L. Li, Y. Sun, C.J. Cui, Y. Zhang, Y. Zhang, F.S. Zhou, X.Y. Jiang, Anticoagulant hydrogel tubes with poly(epsilon-caprolactone) sheaths for small-diameter vascular grafts, Adv Healthc Mater 10 (2021), 2100839.
[44] W.C. Yao, H.B. Gu, T. Hong, Y. Wang, S.H. Chen, X.M. Mo, W.Y. Li, C.S. Wang, T. H. Zhu, S.Y. Lu, A bi-layered tubular scaffold for effective anti-coagulant in vascular tissue engineering, Mater. Des. 194 (2020), 108943.
[45] H. Wang, Y. Feng, H. Zhao, R. Xiao, J. Lu, L. Zhang, J. Guo, Electrospun hemocompatible PU/gelatin-heparin nanofibrous bilayer scaffolds as potential artificial blood vessels, Macromol. Res. 20 (2012) 347–350.
[46] Q.H. Jin, Y. Fu, G.L. Zhang, L. Xu, G.Z. Jin, L.F. Tang, J.H. Ju, W.X. Zhao, R.X. Hou, Nanofiber electrospinning combined with rotary bioprinting for fabricating small-diameter vessels with endothelium and smooth muscle, Compos. B Eng. 234 (2022), 109691.
[47] J.P. Chen, S. Wu, Study on EDTA-chelated copper adsorption by granular activated carbon, J Chem Technol Biot 75 (2000) 791–797.
[48] R.S. Diaz, J.R. Park, L.L. Rodrigues, P.D. Dalton, E.M. De-Juan-Pardo, T. R. Dargaville, Highly elastic scaffolds produced by melt electrowriting of poly(L-lactide-co-epsilon-caprolactone), Adv Mater Technol 7 (2022), 2100508.
[49] B. Pant, M. Park, S.J. Park, Drug delivery applications of core-sheath nanofibers prepared by coaxial electrospinning: a review, Pharmaceutics 11 (2019) 305.
[50] P.L. Fox, C. Mukhopadhyay, E. Ehrenwald, Structure, oxidant activity, and cardiovascular mechanisms of human ceruloplasmin, Life Sci. 56 (1995) 1749–1758.
[51] J. Beurton, A. Boudier, A.B. Seabra, N.E. Vrana, I. Clarot, P. Lavalle, Nitric oxide delivering surfaces: an overview of functionalization strategies and efficiency progress, Adv Healthc Mater 11 (2022), 2102692.
[52] Q. Song, L. Li, K. Xiong, W. Tian, J. Lu, J. Wang, N. Huang, Q. Tu, Z. Yang, A facile dopamine-mediated metal-catecholamine coating for therapeutic nitric oxide gas interface-catalytic engineering of vascular devices, Biomater. Sci. 7 (2019) 3741–3750.
[53] G.N. Hannan, B.R. McAuslan, Modulation of synthesis of specific proteins in endothelial cells by copper, cadmium, and disulfiram: an early response to an angiogenic inducer of cell migration, J. Cell. Physiol. 111 (1982) 207–212.
[54] G.F. Hu, Copper stimulates proliferation of human endothelial cells under culture, J. Cell. Biochem. 69 (1998) 326–335.
[55] E.C. Filipe, M. Santos, J.C. Hung, B. Lee, N.J. Yang, A. Chan, M. Ng, J. Rnjak-Kovacina, S.G. Wise, Rapid endothelialization of off-the-shelf small diameter silk vascular grafts, JACC Basic Transl Sci 3 (2018) 38–53.
[56] R.F. Luo, Y.J. Liu, H. Yao, L. Jiang, J. Wang, Y.J. Weng, A.S. Zhao, N. Huang, Copper-incorporated collagen/catechol film for in situ generation of nitric oxide, ACS Biomater. Sci. Eng. 1 (2015) 771–779.
[57] M. Magaraggia, A. Visona, A. Furlan, A. Pagnan, G. Miotto, G. Tognon, G. Jori, Inactivation of vascular smooth muscle cells photosensitised by liposome-delivered Zn(II)-phthalocyanine, J. Photochem. Photobiol., B 82 (2006) 53–58.
[58] B.B. Ma, G.Z. Liang, F.X. Zhang, Y.Z. Chen, H. Zhang, Effect of hydrogen sulfide on restenosis of peripheral arteries after angioplasty, Mol. Med. Rep. 5 (2012) 1497–1502.
[59] G.D. Yang, K. Cao, L.Y. Wu, R. Wang, Cystathionine gamma-lyase overexpression inhibits cell proliferation via a H_2S-dependent modulation of ERK1/2 phosphorylation and p21(Cip/WAK-1), J. Biol. Chem. 279 (2004) 49199–49205.
[60] G. Yang, L.Y. Wu, R. Wang, Pro-apoptotic effect of endogenous H_2S on human aorta smooth muscle cells, Faseb. J. 20 (2006) 553–555.
[61] X.F. Hao, W.W. Gai, F. Ji, J.D. Zhao, D.D. Sun, F. Yang, H.X. Jiang, Y.K. Feng, Bovine serum albumin-based biomimetic gene complexes with specificity facilitate rapid re-endothelialization for anti-restenosis, Acta Biomater. 142 (2022) 221–241.
[62] R. Wang, The gasotransmitter role of hydrogen sulfide, Antioxidants Redox Signal. 5 (2003) 493–501.
[63] L. Li, P. Rose, P.K. Moore, Hydrogen sulfide and cell signaling, Annu. Rev. Pharmacol. Toxicol. 51 (2011) 169–187.
[64] M.L. Lo Faro, B. Fox, J.L. Whatmore, P.G. Winyard, M. Whiteman, Hydrogen sulfide and nitric oxide interactions in inflammation, Nitric Oxide 41 (2014) 38–47.
[65] B. Geng, J.H. Yang, Y.F. Qi, J. Zhao, Y.Z. Pang, J.B. Du, C.S. Tang, H_2S generated by heart in rat and its effects on cardiac function, Biochem. Biophys. Res. Commun. 313 (2004) 362–368.
[66] B.L. Predmore, D. Julian, A.J. Cardounel, Hydrogen sulfide increases nitric oxide production from endothelial cells by an Akt-dependent mechanism, Front. Physiol. 2 (2011) 104.
[67] M. Kida, T. Sugiyama, T. Yoshimoto, Y. Ogawa, Hydrogen sulfide increases nitric oxide production with calcium-dependent activation of endothelial nitric oxide synthase in endothelial cells, Eur. J. Pharmaceut. Sci. 48 (2013) 211–215.
[68] C. Szabo, Hydrogen sulfide, an enhancer of vascular nitric oxide signaling: mechanisms and implications, Am. J. Physiol. Cell Physiol. 312 (2017) C3–C15.
[69] D. Wu, Q. Hu, Y. Xiong, D.Q. Zhu, Y.C. Mao, Y.Z. Zhu, Novel H_2S-NO hybrid molecule (ZYZ-803) promoted synergistic effects against heart failure, Redox Biol. 15 (2018) 243–252.
[70] X. Gong, X. Zhao, B. Li, Y. Sun, M. Liu, Y. Huang, X. Jia, J. Ji, Y. Fan, Quantitative studies of endothelial cell fibronectin and filamentous actin (F-Actin) coalignment in response to shear stress, Microsc. Microanal. 23 (2017) 1013–1023.
[71] X.X. Chen, L. Feng, H. Jin, Constant or fluctuating hyperglycemias increases cytomembrane stiffness of human umbilical vein endothelial cells in culture: roles of cytoskeletal rearrangement and nitric oxide synthesis, BMC Cell Biol. 14 (2013) 22.
[72] T.R. Dunkern, M. Paulitschke, R. Meyer, R. Büttemeyer, R. Hetzer, G. Burmester, M. Sittinger, A novel perfusion system for the endothelialisation of PTFE grafts under defined flow, Eur J Vasc Endovasc 18 (1999) 105–110.
[73] L.L. Sun, X.F. Li, T. Yang, T. Lu, P.C. Du, C.Q. Jing, Z.G. Chen, F. Lin, G.A. Zhao, L. Zhao, Construction of spider silk protein small-caliber tissue engineering vascular grafts based on dynamic culture and its performance evaluation, J. Biomed. Mater. Res. 111 (2023) 71–87.
[74] A. Dardik, A. Liu, B.J. Ballermann, Chronic in vitro shear stress stimulates endothelial cell retention on prosthetic vascular grafts and reduces subsequent in vivo neointimal thickness, J. Vasc. Surg. 29 (1999) 157–167.
[75] R. Wallin, N. Wajih, G.T. Greenwood, D.C. Sane, Arterial calcification: a review of mechanisms, animal models, and the prospects for therapy, Med. Res. Rev. 21 (2001) 274–301.
[76] T. Sugiura, S. Tara, H. Nakayama, T. Yi, Y.U. Lee, T. Shoji, C.K. Breuer, T. Shinoka, Fast-degrading bioresorbable arterial vascular graft with high cellular infiltration inhibits calcification of the graft, J. Vasc. Surg. 66 (2017) 243–250.
[77] H. Yao, Z. Sun, G. Zang, L. Zhang, L. Hou, C. Shao, Z. Wang, Epidemiological research advances in vascular calcification in diabetes, J. Diabetes Res. (2021), 4461311.
[78] E. Ishimura, S. Okuno, H. Taniwaki, A. Kizu, T. Tsuchida, A. Shioi, T. Shoji, T. Tabata, M. Inaba, Y. Nishizawa, Different risk factors for vascular calcification in end-stage renal disease between diabetics and nondiabetics: the respective importance of glycemic and phosphate control, Kidney Blood Press. Res. 31 (2008) 10–15.
[79] P. Aghagolzadeh, R. Radpour, M. Bachtler, H. van Goor, E.R. Smith, A. Lister, A. Odermatt, M. Feelisch, A. Pasch, Hydrogen sulfide attenuates calcification of vascular smooth muscle cells via KEAP1/NRF2/NQO1 activation, Atherosclerosis 265 (2017) 78–86.
[80] E. Zavaczki, V. Jeney, A. Agarwal, A. Zarjou, M. Oros, M. Katkó, Z. Varga, G. Balla, J. Balla, Hydrogen sulfide inhibits the calcification and osteoblastic differentiation of vascular smooth muscle cells, Kidney Int. 80 (2011) 731–739.
[81] Y. Higashi, Roles of oxidative stress and inflammation in vascular endothelial dysfunction-related disease, Antioxidants 11 (2022) 1958.
[82] Y. Zhu, X. Xian, Z. Wang, Y. Bi, Q. Chen, X. Han, D. Tang, R. Chen, Research progress on the relationship between atherosclerosis and inflammation, Biomolecules 8 (2018) 80.
[83] A. Martelli, E. Piragine, E. Gorica, V. Citi, L. Testai, E. Pagnotta, L. Lazzeri, N. Pecchioni, V. Ciccone, R. Montanaro, L. Di Cesare Mannelli, C. Ghelardini, V. Brancaleone, L. Morbidelli, V. Calderone, The H_2S-donor erucin exhibits protective effects against vascular inflammation in human endothelial and smooth muscle cells, Antioxidants 10 (2021) 961.
[84] K.K. Zimmermann, S.G. Spassov, K.M. Strosing, P.M. Ihle, H. Engelstaedter, A. Hoetzel, S. Faller, Hydrogen sulfide exerts anti-oxidative and anti-inflammatory effects in acute lung injury, Inflammation 41 (2018) 249–259.
[85] A. Tedgui, Z. Mallat, Anti-inflammatory mechanisms in the vascular wall, Circ. Res. 88 (2001) 877–887.
[86] Q. Zhang, L.J. Wang, Y. Yin, J. Shen, J. Xie, J. Yuan, Hydrogen sulfide releasing hydrogel for alleviating cardiac inflammation and protecting against myocardial ischemia-reperfusion injury, J. Mater. Chem. B 10 (2022) 5344–5351.
[87] A. Martelli, L. Testai, V. Citi, A. Marino, I. Pugliesi, E. Barresi, G. Nesi, S. Rapposelli, S. Taliani, F. Da Settimo, M.C. Breschi, V. Calderone, Arylthioamides as H_2S donors: L-cysteine-activated releasing properties and vascular effects in vitro and in vivo, ACS Med. Chem. Lett. 4 (2013) 904–908.
[88] X.X. Jin, Y.F. Wang, J. Yuan, J. Shen, Extraction, characterization, and NO release potential of keratin from human hair, Mater. Lett. 175 (2016) 188–190.
[89] H.W. Yu Zhao, Ming Xian, Cysteine-activated hydrogen sulfide (H_2S) donors, J. Am. Chem. Soc. 133 (2010) 15–17.